SECTION D

Geology of the El Galeno and Michiquillay Cu-Au-Mo deposits and a comparison with the Au-rich Minas Conga porphyry deposit in the Cajamarca mining district, northern Peru

Section D. Geology of the El Galeno and Michiquillay Cu-Au-Mo deposits and a comparison with the Au-rich Minas Conga porphyry deposit in the Cajamarca mining district, northern Peru.

D.1 Abstract

El Galeno and Michiquillay are Miocene Cu-Mo-Au porphyry-related deposits located in the Au-rich Cajamarca district of northern Peru. The El Galeno deposit (486 Mt at 0.57 % Cu, 0.14 g/t Au and 150 ppm Mo) is associated with multiple dioritic intrusions hosted within Lower Cretaceous quartzites and shales. Emplacement of the porphyry stocks (17.5 – 16.5 Ma) in a hanging wall anticline was structural controlled by oblique faults superimposed on early WNW-trending fold-thrust structures. Early K-feldspar-biotite-magnetite (potassic) alteration was associated with pyrite and chalcopyrite precipitation. A quartz-magnetite assemblage that occurs at depth has completely replaced potassically-altered rocks. Late- and post-mineralisation stocks are spatially and temporally related to a weak quartz-muscovite (phyllic) alteration. High Au grades are associated with early intrusive phases located near the centre of the deposit. Highest grade Cu (~0.9 % Cu) is mostly associated with a supergene enrichment blanket, whilst high Mo grades are restricted to contacts with the sedimentary rocks. The Michiquillay Cu-Au-Mo deposit (631 Mt at 0.69% Cu, 0.15 g/t Au, 100-200 ppm Mo) is associated with a Miocene (19.8 Ma) dioritic complex that was emplaced within the hanging wall of a back thrust fault. The intrusive complex is hosted in quartzites and limestones. The NE-trending deposit is crosscut by NNW-trending prospect-scale faults that influenced both alteration and metal distribution. In the SW and NE of the deposit, potassic alteration zones contain moderate hypogene grades (0.14 g/t Au and 0.8 % Cu) and are characterised by chalcopyrite and pyrite mineralisation. The core of the deposit is defined by a lower grade (0.08 g/t Au and 0.57 % Cu) phyllic alteration that overprinted early potassic alteration. Michiquillay contains a supergene enrichment blanket of 45 to 80 m thickness with an average Cu grade of 1.15 %, which is overlain by a deep leached cap (up to 150 m). In contrast to these Cu-Au-Mo deposits, the Au-rich Minas Conga deposit (~23.2 Ma) contains a well-developed potassic alteration associated with strong bornite + chalcopyrite mineralisation.

Sulphide Pb isotope ratios from these Cu-Au-Mo deposits and the Au-rich Minas Conga deposit scatter slightly but suggest a common mantle-dominated source. Similarities between these deposits include age (early-middle Miocene), intrusive rock type (dioritic) and metal source (deep mantle). Despite these similarities, results from this study suggest variation in metal grade between the Au-rich and hybrid-type deposits resulted from a combination of processes. These include temperature and oxygen fugacity conditions during hypogene mineralisation, late fluid flow resulting in a well-developed phyllic alteration zone, precipitation of ubiquitous hydrothermal magnetite, and complexity of intrusive history.

D.2 Introduction

The Cajamarca mining district, located in northern Peru, has one of the largest gold inventories in South America with the economic high-sulphidation Yanacocha Au mine, plus several smaller Au epithermal and porphyry Cu-Au deposits that include the Minas Conga (Au-Cu), Michiquillay (Cu-Au-Mo) and El Galeno (Cu-Au-Mo) prospects. Gold reserves for Minera Yanacocha are approximately 36.6 Moz (Newmont, 2002) and the three intrusion-related systems have a combined mineral resource in excess of 1600 Mt (Llosa and Veliz, 2000; McInnes, 1997; Cordova and Hoyos, 2000). Several barren intrusions of older or similar age and composition also crop out in the region. To the north of the Cajamarca district are a number of high-sulphidation Au deposits that include Sipán, La Zanja, Tantahuatay, and the porphyry-skarn-manto polymetallic Hualgayoc district (Fig. 1).

Previous work at mineralised centres in the Cajamarca region includes several studies at the Michiquillay deposit by Laughlin *et al*. (1968), Hollister and Sirvas (1974), and reports by the Metal Mining Agency, Japan International Cooperation Agency (1975) and McInnes (1997). Turner (1997, 1999) discussed the volcanic setting and styles of mineralisation of the Yanacocha deposits as well as other high-sulphidation systems (Sipán, La Zanja and Tantahuatay). Recent work by Longo (2000) provided a detailed discussion on the San Jose-Charachugo-Chaquicocha gold trend within the Yanacocha district, whilst Llosa and Veliz (2000) documented alteration and

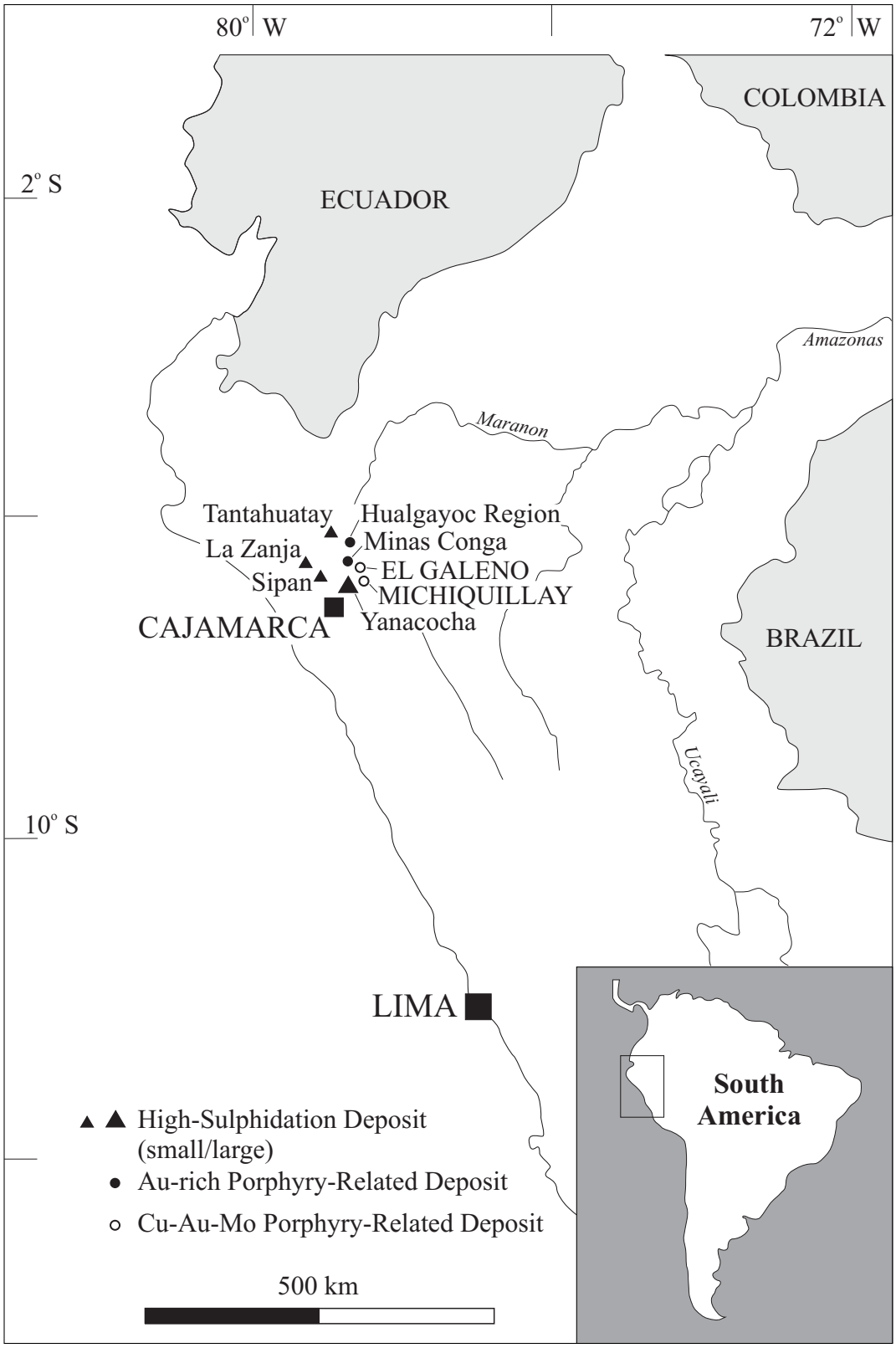

Fig. 1. Map of Peru showing the major mineralised centres near the township of Cajamarca.

mineralisation styles at the Au-Cu Minas Conga prospect. Unpublished reports (Hammond, 1998; Garcia, 1999; Sillitoe, 2000a; Davies, 2000) and published work by Cordova and Hoyos (2000) describe the geology of El Galeno.

This section presents a detailed geological description of the El Galeno (Cu-Mo-Au) prospect with emphasis on documentation of the relative timing of the different intrusive phases, as well as characterisation of the alteration, mineralisation and vein infill paragenesis. Revised intrusive, structural, alteration and mineralisation data from the Michiquillay prospect are also presented. New Pb isotope compositions for sulphide minerals from mineralised intrusions at the El Galeno, Michiquillay, Minas Conga and Yanacocha deposits are also presented. Finally, El Galeno and Michiquillay are compared with the relatively well-documented Au-rich Minas Conga porphyry complex.

D.3 Regional Geological Setting

The Cajamarca district is located in the Western Cordillera of northern Peru. The region is characterised by deformed Cretaceous marine sedimentary rocks that have undergone several phases of compressive deformation since Palaeogene time and been intruded by multiple magmatic phases (Fig. 2). Hydrothermal and mineralisation events were temporally related to two major magmatic episodes, i.e. early to middle Miocene porphyry Cu-Au-Mo formation and late Miocene epithermal activity (refer to Section A). The geological setting of northern Peru and the Cajamarca region is outlined in Benavides (1956), Reyes (1980), Wilson (1985a, 1985b), Cobbing *et al*., (1981), Turner (1997) and Wilson (2000).

D.3.1 Cretaceous to Oligocene Rocks

The oldest rocks that crop out in the Cajamarca region are a thick package of Lower- to Upper-Cretaceous platform sedimentary rocks. These sedimentary units include Lower-Cretaceous sandstone and quartzite sequences at the base of the package that fine upward to Upper-Cretaceous limestone, marl and shale sequences (Benavides, 1956). Intense folding and thrusting of the marine sediments from 59 to 55 Ma resulted

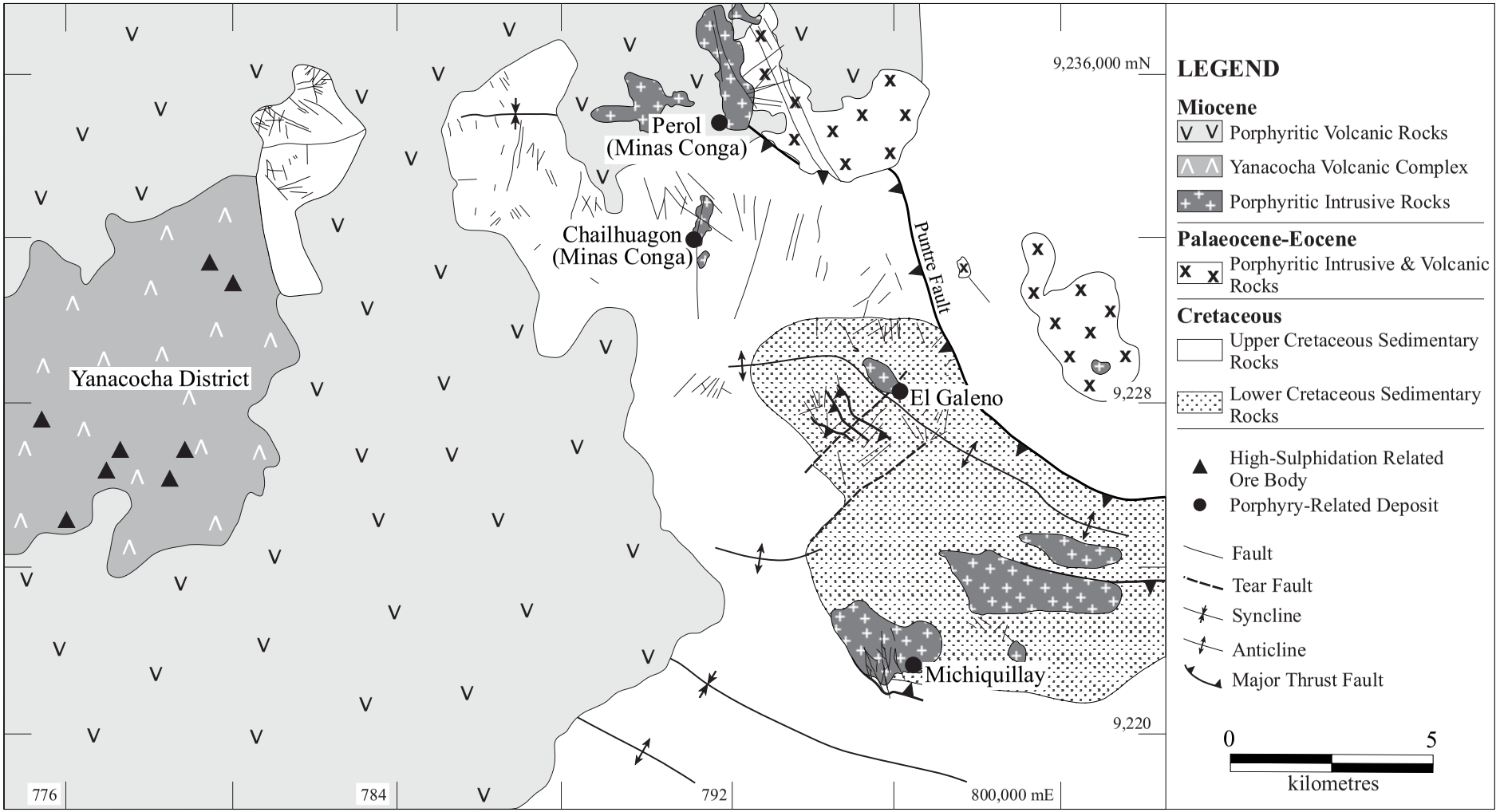

Fig. 2. Simplified geological map of the Cajamarca region showing the distribution of the major mineralised centres (modified from Reyes, 1980).

in emergence of the Cretaceous sedimentary units and development of open, upright folds and imbricate thrust sheets (Mégard, 1984, 1987).

The deformed sedimentary rocks are unconformably overlain by predominantly basaltic to andesitic volcanic sequences known as the Llama Formation (Noble *et al*., 1990; Atherton *et al*., 1985). The Lower Llama Volcanic Sequence forms an aerially-extensive volcanic succession that range in age from 54.8 to 42.6 Ma (Atherton *et al*., 1985; Noble *et al*., 1990; Section A). Intrusions in the Minas Conga, Cerro Perol and Cruz Conga regions indicate several stocks were emplaced between 57 and 43 Ma (Llosa *et al*., 1996; Section A).

D.3.1 Miocene Rocks

Early to middle Miocene magmatic units (23.2 – 15.8 Ma) are composed of intermediate, calc-alkaline porphyritic intrusive and volcanic rocks that contain plagioclase, mafic ± quartz phenocrysts. Geochronological studies of mineralised porphyry systems indicate emplacement, main stage alteration and mineralisation at these centres occurred during this magmatic interval (Llosa *et al*., 1996; Section A). Coeval barren porphyritic stocks of similar composition display weak propylitic alteration (Section A and C). The youngest intrusive age for this second magmatic interval is defined by an $^{40}Ar/^{39}Ar$ date of 16.5 Ma from a post-mineralisation intrusion at El Galeno (Section A), whilst the Upper Llama Volcanic Sequence has been dated at 15.8 Ma also using $^{40}Ar/^{39}Ar$ age dating (Turner, 1997). An interval from *ca*. 16 to 12 Ma is defined by an apparent decrease in magmatic and deformation activity in the Cajamarca region. However, the period between 14 and 10 Ma corresponded with major magmatic and hydrothermal activity in the polymetallic Hualgayoc district to the north (Macfarlane *et al*., 1994). Several mineralised centres developed in the Hualgayoc region during this period, including those at Cerro Corona and Tantahuatay (Fig. 1).

Deposition of andesitic lava flows of the Regalado Formation (12.3 to 11.6 Ma; Turner, 1997) represented the initiation of middle to late Miocene magmatic activity. Economically, the most productive interval for the Cajamarca region occurred between 12 and 10 Ma with formation of the high-sulphidation Yanacocha Au deposit. Main stage mineralisation at Yanacocha took place between 11.5 and 10.9 Ma (Turner, 1997).

Magmatic and hydrothermal activity in the region ceased in the late Miocene (~8 Ma) with the onset of a shallowing subduction zone (Gutscher *et al*., 1999).

D.4 Regional Structure

The Cajamarca area is located within the southern part of the Huancabamba Deflection zone where Andean structural fabric rotates from NNW to near E-W (Mégard, 1984). The reader is referred to Section B of this thesis for a detailed structural synthesis of the Cajamarca region.

Structural features observed in the deformed Cretaceous sedimentary rocks include large wavelength (>5 km) open folds that plunge gently WNW or ESE. In the northeastern part of the study area, a thrust fault known as the Puntre Fault is spatially associated with numerous magmatic units of both Palaeogene and Miocene age (Fig. 2). The thrust fault displays a major deflection in trend from near E-W to near N-S (see below). To the east and west of the deflection, the Puntre fault has a NW trend consistent with local regional structures. Faults and fractures in the Cretaceous sedimentary rocks are generally subvertical with dominantly normal slip ranging from a few to tens of metres. In the study area, subvertical fault planes plot in three general domains, which include N-S, E-W and ESE-trending. N-striking faults are the most abundant orientation recognised from aerial-photo interpretation (Section B).

D.5 El Galeno

El Galeno is a Cu-Au-Mo porphyry deposit with an estimated geological resource of 486 Mt at 0.57 % Cu, 0.14 g/t Au and 150 ppm Mo (Cordova and Hoyos, 2000). It is exposed at an altitude between 3,850 and 4,100 m. Multiple intrusive stocks were emplaced between *ca*. 17.50 and 16.53 Ma (Section A). The intrusions are hosted by folded Lower Cretaceous sedimentary rocks and were emplaced in a hanging wall anticline (Fig. 3). Mineralisation is characterised a hypogene zone overlain by a supergene enrichment blanket up to 120 m thick. Several unmineralised gabbroic dykes crop out to the southwest and northwest of the mineralised centre, and display weak to

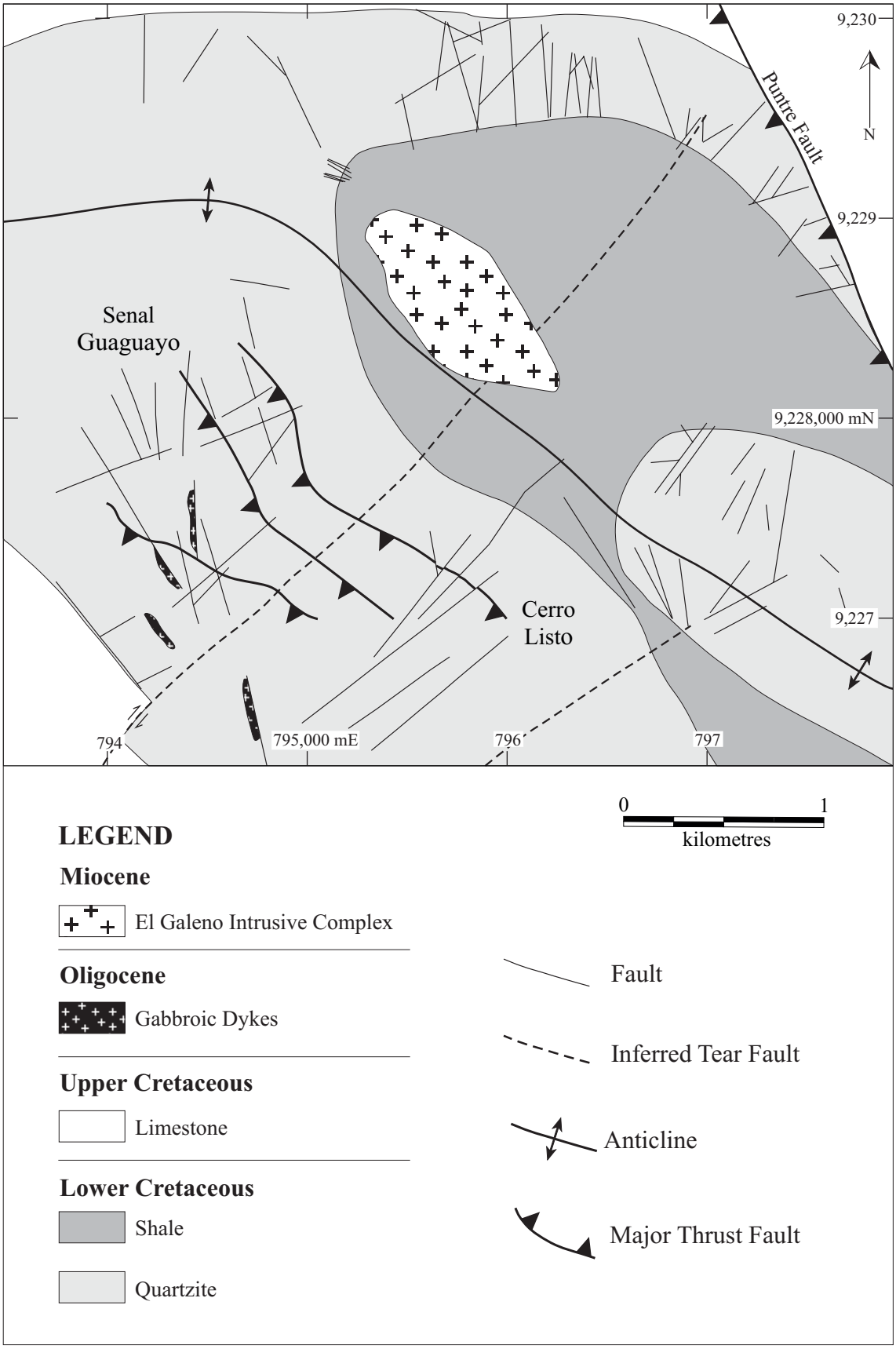

Fig. 3. Simplified structural map of El Galeno displaying the localisation of the intrusive complex within the hanging wall of the Puntre Fault and at the intersection of the NW-plunging El Galeno Anticline and a NE-trending dextral tear fault.

moderate chlorite alteration. The dykes intruded both subvertical N- to NW-trending fault planes and steeply dipping bedding planes. $^{40}Ar/^{39}Ar$ age dating of hornblende phenocrysts from a gabbroic dyke (S-16) yielded an approximate age of 29.4 ± 1.4 Ma (Section A), indicating the dykes are Oligocene in age and intruded prior to emplacement of the El Galeno porphyry complex.

D.5.1 Lithology

Field evidence indicates that the El Galeno porphyry complex is mainly hosted within quartzite and siltstone sedimentary units (Fig. 4). Observed contacts between intrusions and sedimentary host rocks are subvertical. Furthermore, drilling indicates the intrusive complex does not extend laterally beyond the outcrop limit (Appendix D1). The intrusive complex is elliptical in shape, ~1250 m in length by 600 m wide, and its long axis is oriented NW-SE. This orientation is roughly parallel to the WNW trend of the hanging wall anticline (El Galeno Anticline) that hosts the mineralised centre. The complex comprises at least four intrusive phases (Fig. 5), three of which are identifiable in outcrop and the other from drill core logging (Appendix D1).

P1 Porphyry - The oldest intrusive phase is a crowded medium-grained porphyritic diorite mostly composed of euhedral to subhedral plagioclase, with less abundant euhedral biotite, hornblende and rounded quartz phenocrysts (Fig. 6a). Plagioclase phenocrysts (An_{44-46}; 35-45 vol. %) range between 0.3 and 5.0 mm in length and show multiple twinning plus oscillatory zoning. Magmatic biotite and hornblende phenocrysts (1 vol. %) of 0.5 to 2.0 mm length are mostly replaced by secondary biotite. This is the largest body of the four recognised phases and later intrusive units were emplaced toward the core of this stock.

P2 Porphyry - The second intrusive phase is also a porphyritic diorite but texturally heterogeneous. It is dominantly characterised by a crowded porphyritic texture (Fig. 6b) with fine-grained plagioclase (0.5-1.0 mm; An_{42-60}) and less abundant rounded quartz grains, but varies to a medium-grained (1.5-3.0 mm) weakly porphyritic rock. Backscattered images of plagioclase phenocrysts illustrate compositional zoning (Fig. 5 in Section C). Phenocrysts show similar characteristics to magmatic grains in the

Fig. 4. Geological map of El Galeno with the major lithological units and prospect-scale structures. Outcrops of the intrusive complex were mostly created by road construction. Also, shown are the outer limits of Cu grade zones and the locations of drill core logged.

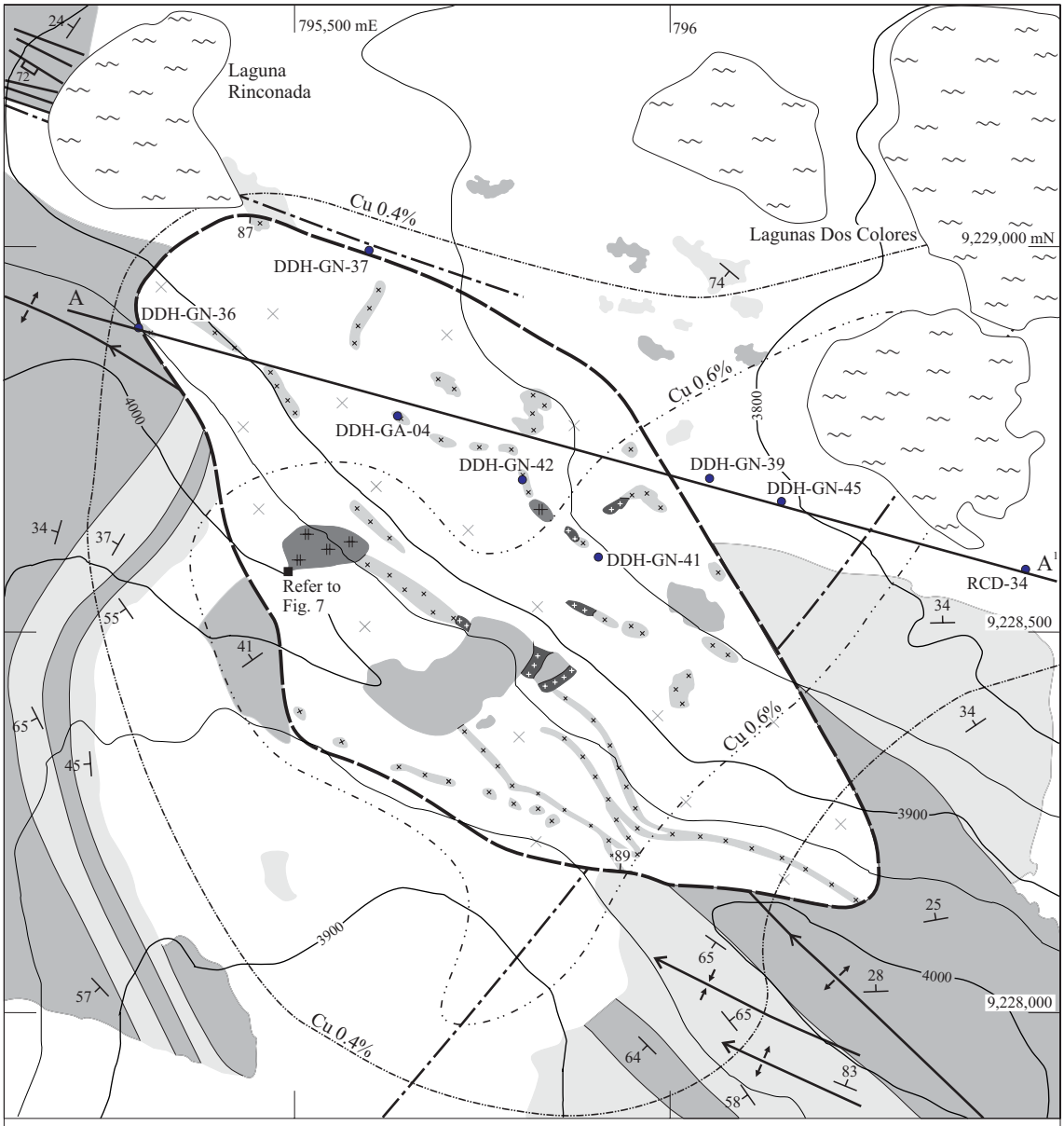

0 metres 250

N

LEGEND

Pleistocene

- Alluvial Gravels

Miocene

El Galeno Porphyry Complex
- P3 Porphyry
- P2 Porphyry
- P1 Porphyry

Lower Cretaceous

- Quartzite
- Sandstone & Shale

- Lake
- 3900 Topography (C.I. 50 m)
- A A' Drill Core Cross-Section

- 53 Strike and dip of bedding
- 23 Trend and plunge of anticline
- 26 Trend and plunge of syncline
- Trend and plunge of fault
- Inferred fault
- Outcrop limit of intrusive complex
- Outer limit of Cu grades >0.6%
- Outer limit of Cu grades 0.6-0.4%

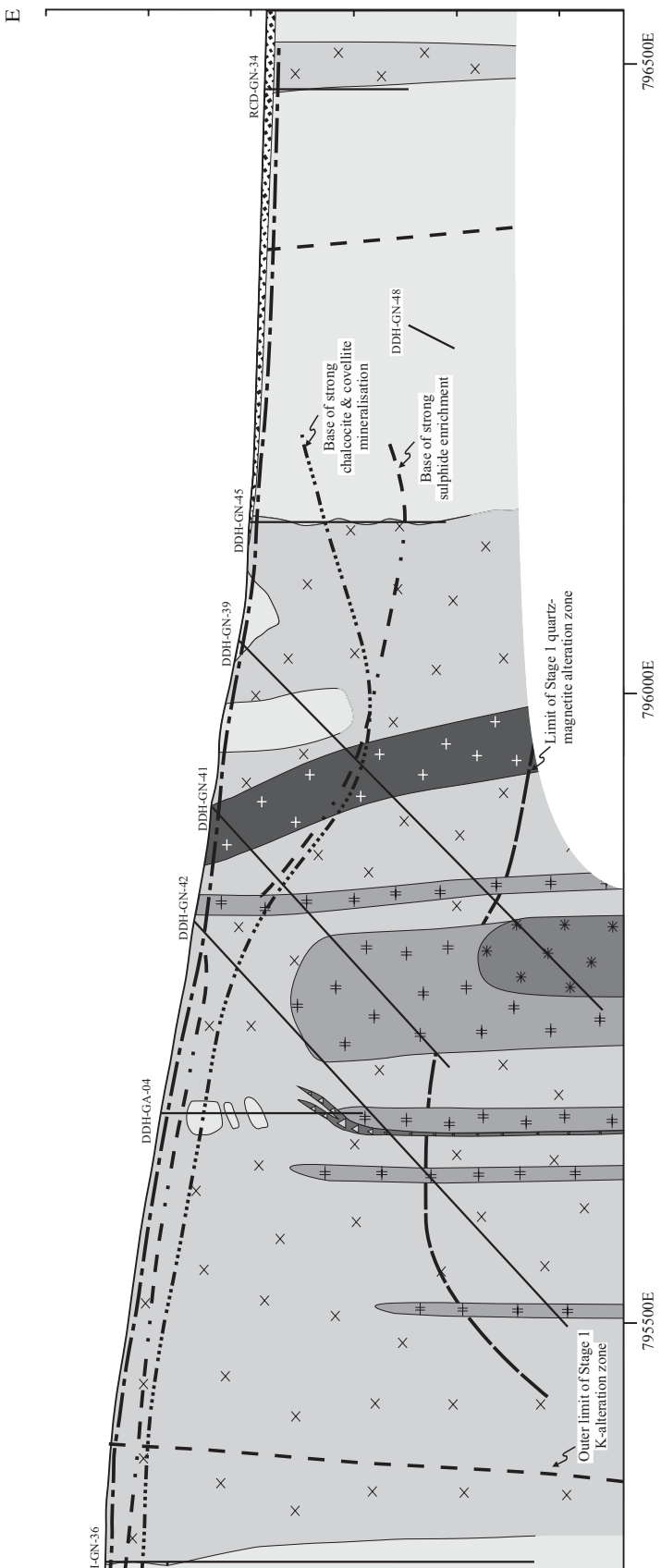

Fig. 5. Near E-W section through the El Galeno porphyry complex showing the distribution of the major lithological units and outer limits of alteration assemblages [based on drill core logging by Sillitoe (2000a) and the author (Appendix D1)]. The lower limits of the leached cap, chalcocite-covellite zone and sulfide enrichment blanket are also shown.

Fig. 6. Photographs of the different intrusive phases within the Galeno complex. (a) P1 porphyry composed dominantly of plagioclase (PL), hornblende (Hbl), biotite (Bt) and quartz (Qtz) phenocrysts. Plagioclases (yellow-orange colour) have been partially replaced by muscovite and illite. DDH-GN-42 96.6 m. (b) P2 porphyry with a medium to fine-grained crowded porphyritic texture consisting of plagioclase, biotite phenocrysts and fine-grained hornblende. Crosscutting quartz - K-feldspar veins (pink) and minor sulphides (dusty yellow centre) are related to dark K-feldspar-biotite alteration that is overprinted by weak propylitic alteration (light green spots upper left). DDH-GN-39 214 m. (c) P3 porphyry with coarse-grained plagioclase, biotite and hornblende and quartz phenocrysts. DDH-GN-42 246 m. (d) Biotised MBx porphyry with plagioclase (PL) and biotite (Bt) phenocrysts. MBx contains fragments of altered and mineralised P3 porphyry. Dark, fine-grained selvages composed of hydrothermal biotite rim some fragments. DDH-GN-39 400 m.


THE IMAGES ON THIS PAGE HAVE BEEN REMOVED DUE TO
COPYRIGHT RESTRICTIONS

P1 porphyry. Hydrothermal biotite from this intrusion yielded an age of 17.5 ± 0.3 Ma using $^{40}Ar/^{39}Ar$ (Section A).

P3 Porphyry – The P3 porphyry is a coarse-grained crowded quartz-diorite porphyry with euhedral plagioclase, quartz, biotite and hornblende phenocrysts (Fig. 6c). Plagioclase phenocrysts (An_{42-51}; 30-35 vol. %) display oscillatory zoning and range in length from 1.0 up to 8.0 mm. Rounded quartz phenocrysts are 2.0 to 10.0 mm in length and may have minor embayments. Euhedral biotite books (6 vol. %) range from 1.0 to 10.0 mm in length and hornblende (~3 vol. %) phenocrysts are between 1.0 to 5.0 mm. This porphyry contains rare xenoliths of quartz-magnetite altered fragments. In drill core the occurrence of these intrusions is sporadic, varies in thickness from a few metres to tens of metres and was mainly intersected toward the centre of the P1 porphyry (Fig. 5). In outcrop (Fig. 4), contacts of a P3 porphyry body are near vertical (Fig. 7) from which it is inferred that this intrusive phase occurs as a number of small-sized vertical dykes.

P3 Porphyritic Breccia - Hydrothermal breccias (P3 porphyritic breccia) are located along the contacts of some of the P3 porphyry bodies (Fig. 5). Xenoliths observed within the hydrothermal breccia include angular to subrounded quartz and quartz-magnetite vein fragments that range in size from millimetres up to several centimetres (refer to Fig. 11a). The matrix is dominantly composed of quartz, muscovite and pyrite.

Thin (0.3-2.0 m wide) dioritic dykes are characterised by crowded porphyritic texture with abundant feldspar (0.6–2.5 mm) and minor mafic phenocrysts set within a light grey feldspathic groundmass. The dykes were not observed in outcrop and rarely intersected in drill core. The dykes are considered to have formed late in the evolution of the intrusive complex, probably following emplacement of the third intrusive phase. However, their exact timing is unclear.

MBx Porphyry - The youngest intrusive phase is a magmatic breccia that is weakly porphyritic, with phenocrysts and xenoliths set in a feldspar-rich matrix (Fig. 6d). Euhedral plagioclase phenocrysts (An_{40-56}; ~10 vol. %; 0.5 to 9.0 mm) show multiple twinning textures and generally contain sieve-textured rims that suggest

Fig. 7. Photograph of a quartz-muscovite altered P3 porphyritic dyke that has intrude the P1 porphyry. Note the low vein density of the dyke compared to the earlier porphyry.

plagioclase instability (refer to insert of Fig. 11b). Biotite books (~2 vol. %) are euhedral and vary from 0.3 to 3.0 mm in size. Rounded quartz phenocrysts (~1 vol. %) are ~3.0 mm in length and acicular hornblende grains (0.3-2.0 mm) are partially replaced by secondary biotite. This unit was intersected at depth in the northern central part of the P1 porphyry (e.g. drill holes logged in Appendix D1). Xenoliths are generally rounded and range in size from a few to tens of centimetres. Altered and mineralised xenoliths of the previous three intrusive phases are the dominant clasts. Many clasts have thin (~1 mm) fine-grained dark selvages composed of hydrothermal biotite. Magmatic biotite books from this intrusion yielded a $^{40}Ar/^{39}Ar$ plateau age of 16.53 ± 0.18 Ma (Section A).

D.5.2 Structural Geology

El Galeno is situated at the intersection of a hanging wall anticline and a NE-striking tear fault (Fig. 3). The hanging wall anticline, called El Galeno Anticline, has a gentle plunge to the NW ($25^o \rightarrow 303^o$) and is located immediately above the Puntre Thrust fault. The Lower Cretaceous Chimú and Santa Formations in the hanging wall of the fault are juxtaposed against the Middle-Upper Cretaceous Yumagual Formation in the footwall, indicating over 2000 m of reverse offset based on unit thicknesses measured by Benavides (1956). To the east and northwest of the intrusive system, the reverse fault strikes approximately WNW and dips at a low angle (~30^o) to the SSW, suggesting that the fault forms a low-angle thrust ramp. However, to the northeast of the complex the reverse fault deflects in a clockwise direction to near NNW (Fig. 3). Within this NNW-trending zone of the fault, argillic-altered sedimentary rocks have a subvertical dip and display polyphase deformation. These features include early WNW shallowly plunging folds and subhorizontal calcite veins that are both crosscut by later extensional structures including subvertical calcite veins and small-scale normal faults (Section B.4.1). Other features observed in near proximity to the thrust zone include a bend in the hanging wall anticline axis towards the deflection zone and abundant fractures in Goyllarisquizga Group quartzites on the northern limb of the anticline. These features suggest a change from a low-angle frontal ramp, to the east and northwest of El Galeno, to a high-angle oblique ramp within the zone of deflection.

Southwest of the intrusive complex, exposures on Senal Guaguayo contain subvertical normal faults that range from NW- to near E-trending. Displacement along the fault planes varies from roughly two to five metres. Fault breccias and altered Oligocene gabbroic dykes (1–3 m wide) occur along some of these fault planes. Normal faults measured at Cerro Listo have a uniform orientation with a general NE trend and offsets up to 10 m. These subvertical faults are characterised by minor brecciation along fault planes, although gabbroic dykes are noticeably absent at Cerro Listo. Aerial photo interpretation suggests a NE-trending tear fault bisects the valley between topographic peaks of Senal Guaguayo and Cerro Listo (Fig. 3). This tear fault is interpreted to crosscut the El Galeno Anticline.

West of Laguna Rinconada (Fig. 4) a series of small-scale normal faults were observed within the Farrat Formation. These subvertical faults have an approximate E-W strike and display minor (0.5-2.0 m) displacement. Drill cores along strike of these faults (e.g. DDH-GN-37) are strongly fractured and characterised by intense clay alteration to depths in excess of 300 m (Appendix D1). It is inferred that the fault set west of Laguna Rinconada extends into the intrusive centre. The nature and history of this fault with respect to pluton emplacement, controls on mineralisation plus possible post-mineralisation offset is uncertain.

D.5.3 Alteration, Mineralisation and Vein Paragenesis

Four separate alteration events are identifiable at the El Galeno prospect based on drill core logging and petrographic studies. The first of these is temporally and spatially related to the earliest two intrusive phases. P3 porphyry truncates mineralised P1 and P2 porphyries indicating hydrothermal events occurred prior to its emplacement. Altered P3 porphyry is in turn crosscut by P3 hydrothermal breccias, with MBx porphyry containing mineralised xenoliths of all earlier intrusive phases. Alteration assemblages associated with each of the intrusive phases display zoned distributions.

Mineralisation is divided into two main phases, namely hypogene mineralisation, which includes up to three separate stages, and secondly supergene mineralisation (Fig. 8). Hypogene mineralisation occurs in all four generations of

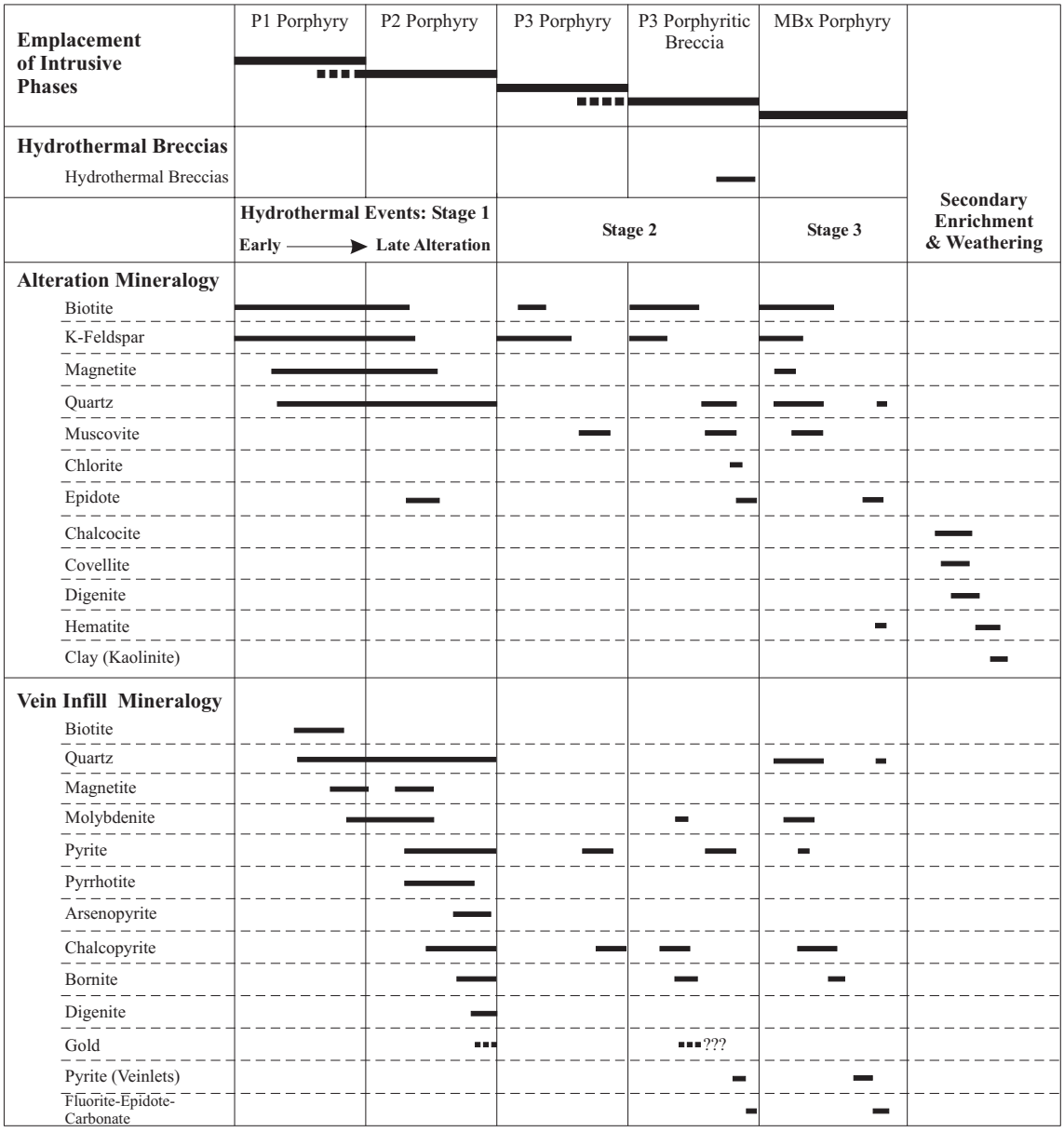

Fig. 8. Alteration and vein paragenesis at El Galeno.

porphyry intrusions as well as extending tens to a few hundreds of metres into the host sedimentary rocks.

Stage 1

Alteration - The oldest and most widespread alteration identified in drill core is observed within the earliest two intrusions. The dominant assemblage consists of K-feldspar and biotite (potassic alteration). This is characterised by replacement of plagioclase phenocrysts by K-feldspar (Fig. 9a), while primary hornblende and biotite phenocrysts are replaced by hydrothermal biotite, plus formation of fine-grained secondary biotite within the matrix. Minor amounts of fine-grained magnetite occur along the rims of altered mafic minerals and disseminated within the matrix. The earliest vein types include biotite-quartz fracture infillings (Fig. 9b), followed by quartz veins of varying thickness (0.5 mm up to 10 cm). The highest density of quartz stockwork is related to this alteration stage and generally extends about 200 m below the current surface (Appendix D1). Stockwork density generally decreases with depth and toward the periphery of the intrusive system, although quartz stockwork locally extends up to 100 m in to the host rocks. Minor silicification and a weak propylitic alteration are also evident along the contact margins with sedimentary host rocks and in localised zones of the P1 porphyry.

Pervasive magnetite-quartz alteration (Fig. 9c) occurs at depth and toward the central zone of the P1 porphyry (Fig. 5). Quartz-magnetite-altered fragments occur as xenoliths in the P3 porphyry, although a weak magnetite alteration is evident along its contacts. These relationships indicate this quartz-magnetite alteration dominantly occurred at depth and prior to emplacement of the third intrusive phase.

Hypogene Sulphides - Hypogene mineralisation identified at El Galeno is both fracture infill and disseminated in character. The earliest mineralisation was molybdenite (Fig. 9d) deposited in re-opened early quartz veins within both the P1 porphyry and host sedimentary rocks. These quartz veins range in thickness from a few millimetres to centimetres. The highest molybdenite abundances occur along the contacts between the host sedimentary rocks and P1 porphyry (Fig. 10a). This oldest mineralisation phase was followed by the deposition of magnetite and pyrite (Fig. 9d) with varying proportions of arsenopyrite and pyrrhotite. Later chalcopyrite (Fig. 9d) and

Fig. 9. Photographs of alteration and mineralisation features at El Galeno. (a) Photomicrograph of a zoned plagioclase phenocryst crosscut and partially replaced by early Stage 1 potassic alteration. (b) Stage 1 early biotite (Bt) vein in the P1 porphyry crosscut by a quartz (Qtz) vein (middle left of image). Thin magnetite (Mag) veins post-date both the biotite and quartz veins. DDH-GN-42 96.6 m. (c) Stage 1 quartz-magnetite alteration crosscut by quartz and quartz-magnetite veins. Magnetite infill of reopened veins and late pyrite (Pyr) veinlets are also evident. DDH-GN-42 465 m. (d) Photomicrograph of Stage 1 mineralisation with early molybdenite, followed by pyrite and finally chalcopyrite. DDH-GN-39 166m. (e) Photomicrograph showing Stage 2 K-feldspar (bottom left to top centre) has partially replaced a plagioclase phenocryst. Fine-grained hydrothermal biotite (pink, top right) also precipitated during this alteration stage. Both of these minerals are partially replaced by muscovite/illite. DDH-GN-41 258 m. (f) Stage 2 pyrite vein with a quartz-muscovite halo in a P3 dioritic dyke. DDH-GN-39 215 m.


THE IMAGES ON THIS PAGE HAVE BEEN REMOVED DUE TO
COPYRIGHT RESTRICTIONS

Fig. 10. Section A-A^{1} showing metal grade distributions. High Au and Cu grades are located in the upper eastern section of the porphyry complex. Moderate Cu grades also occur on the western flank of the complex. High Mo grades are mostly located on the edges of the complex. The quartz-magnetite alteration and late porphyries (P3 and MBx) are poorly mineralised.

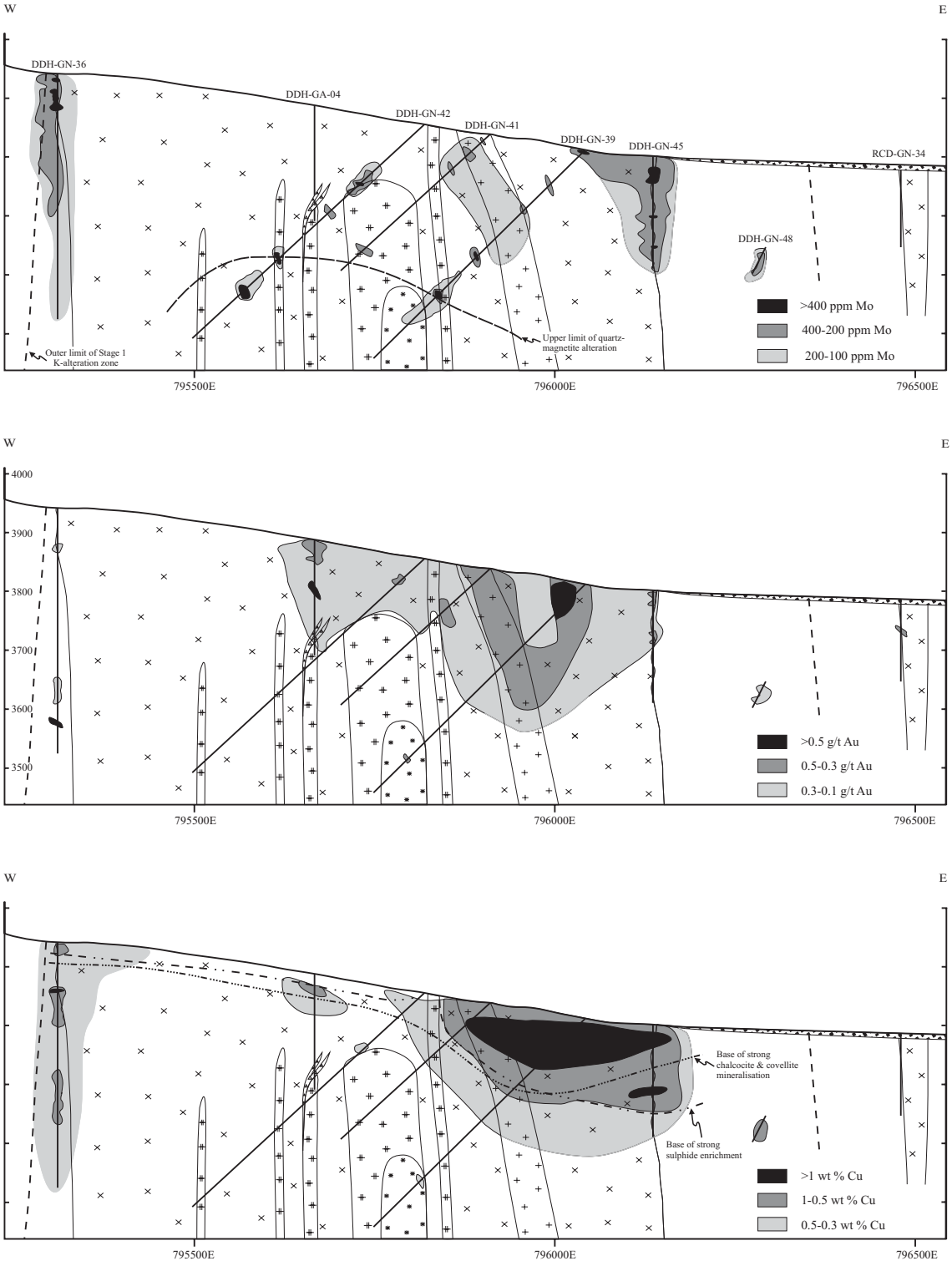

LEGEND

- Recent Alluvium
- MBx Porphyry
- P3 Porphyritic Breccia
- P3 Porphyry
- P2 Porphyry
- P1 Porphyry
- Sedimentary Rock
- Chalcocite-Covellite replacement
- Sulphide enrichment
- Upper limit of quartz-magnetite alteration
- Outer limit of Stage 1 K-alteration and pronounced quartz stockwork

minor amounts of bornite crosscut these earlier phases. These later mineralisation phases are evident in both the P1 and P2 intrusions. Hypogene pyrite, chalcopyrite and molybdenite also extend into the sedimentary host rocks. Based on logging and assay data (Appendix D2), high-grade hypogene zones are associated with intense hydrothermal biotite alteration zones and localised contacts between the host units and P1 porphyry (Fig. 10b-c).

Stage 2

Alteration - The second alteration stage was temporally related to emplacement of the P3 porphyry, P3 hydrothermal breccias and possibly the diorite dykes (Fig. 8). The earliest alteration identified with this stage involved intense K-feldspar replacement of the groundmass and primary plagioclase grains, and hydrothermal biotite replacement of primary mafic minerals. This potassic alteration has a smoky, light grey appearance that is particularly characteristic within P3 porphyries (Fig. 6c). The diorite dykes have a similar alteration assemblage but a slightly darker appearance. Development of new quartz veins and reopening of older veins was also related to this alteration phase. This alteration has a substantially lower vein density than the Stage 1 alteration (Fig. 7; Appendix D1).

A quartz-muscovite/illite ± pyrite (phyllic) alteration assemblage overprints the potassic-silicate alteration and early quartz ± molybdenite veins. The quartz-muscovite/illite alteration is defined by muscovite replacement of feldspar grains (Fig. 9e; Appendix D3), silicification of the groundmass and quartz infill in new or reopened fractures. Weak quartz-muscovite alteration is evident within the first three intrusive phases and dominantly restricted to the upper 150 m of the intrusive centre.

Hypogene Sulphides - Late quartz-muscovite-pyrite veins and thin pyrite veinlets overprint earlier stockwork. The quartz-pyrite veins with muscovite halos (Fig. 9f) are related to the weak phyllic alteration and veins mostly comprise pyrite infill. Minor chalcopyrite, bornite and molybdenite also precipitated along fracture planes. These veins are dominantly found within, or in close proximity, to the third intrusive phase. The P3 hydrothermal breccias have a quartz-muscovite-pyrite matrix with xenoliths of quartz-magnetite (Fig. 11a). This mineralisation event is distinguishable from stage 1 by a substantial decrease in Au, Cu and to a lesser extent Mo, but produced

Fig. 11. Photographs of alteration and mineralisation features at El Galeno. (a) Xenolith fragments of P1, P2, P3 and quartz-magnetite veins in the P3 hydrothermal breccia. The matrix of the breccia dominantly comprises quartz, muscovite and pyrite. DDH-GA-04 192.3 m. (b) Biotised MBx porphyry that contains thin quartz veins related to Stage 3 alteration. These veins have been reopened and infilled with molybdenite (Mo) and chalcopyrite (Ccp). Insert, plagioclase phenocryst with sieved-texture rim. DDH-GN-39 432 m. (c) Phyllic altered MBx porphyry with P1 porphyry fragment. Late pyrite veinlets crosscuts contact between the P1 fragment and MBX porphyry. Fine-grained plagioclase grains have been near completely replaced by muscovite/illite. DDH-GN-39 (435.8 m). (d) Photomicrograph of Stage 3 molybdenite and hematite (Hem; orange-brown). DDH-GN-39 432 m. (e) Photomicrograph of Stage 3 molybdenite, chalcopyrite and bornite (Bn). Late hematite partially replacing the copper-iron sulphide minerals, which are chalcopyrite and bornite. DDH-GN-39 432 m. (f) Chalcopyrite grain rimmed by late chalcocite (Cc) during secondary enrichment. DDH-GN-39 166.1 m.


THE IMAGES ON THIS PAGE HAVE BEEN REMOVED DUE TO
COPYRIGHT RESTRICTIONS

zones with anomalously high Zn and Pb content (see below). Anomalously high Ag, Pb, and Zn grades are also associated with the hydrothermal breccia (Appendix D2). It is inferred that main stage deposition of Au, Cu and Mo occurred prior to emplacement of this phase.

Stage 3

Alteration - The youngest alteration event identified was temporally and spatially related to the emplacement of the final intrusive phase, i.e. MBx porphyry. Alteration is dark grey in appearance (Fig. 11b) and dominantly characterised by intense fine-grained hydrothermal biotitisation of magmatic mafic minerals plus the groundmass. Weak K-feldspar replacement of plagioclase and the groundmass was also associated with this event. Quartz-muscovite-pyrite (phyllic) alteration is evident near contacts between xenoliths and the magmatic breccia. This phyllic alteration is characterised by a high abundance (up to 15 vol. %) of disseminated fine-grained pyrite and intense muscovite replacement of feldspar (Fig. 11c).

Hypogene Sulphides - Several late veining events are temporally related with this alteration phase and contain similar mineralogy to the previous phases. The xenoliths display barren and mineralised veins that terminate at the fragment boundaries, which suggest that this mineralisation phase represents a new hypogene mineral deposition phase. However, as shown below metal grades associated with this intrusive-hydrothermal phase are the lowest of all the mineralising phases.

Sulphide minerals are commonly associated with zones of intense biotite and K-feldspar alteration. Early magnetite precipitation was followed by development of thin (~3 mm), wavy quartz veins. Quartz veins were later reopened and molybdenite, followed by pyrite, then chalcopyrite and bornite were deposited (Fig. 11b-e). These assemblages are crosscut by hairline pyrite veinlets (Fig. 11c). This late stage alteration also involved partial to complete hematite replacement of chalcopyrite and bornite (Fig. 11d-e). This was possibly associated with late fluorite-epidote-carbonate-quartz infill.

Secondary Enrichment & Weathering

Weak clay (argillic) alteration mostly occurs within the upper 10 m of the intrusive complex or zones with abundant fractures. In these zones, relict feldspar and mafic minerals have been replaced by kaolinite (Appendix D3).

Secondary mineralisation is restricted to a supergene blanket that extends *ca.* 120 m below the current surface (Fig. 5; Sillitoe, 2000a). Sulphide minerals present within the supergene blanket include chalcocite and minor covellite. Chalcocite replacement is mostly observed along the rims of both hypogene chalcopyrite and bornite (Fig. 11f). Metal grades within the supergene blanket range from 0.7 up to 1.2 % Cu. These grades are considerably higher than those related to hypogene mineralisation, which generally range between 0.2 and 0.3 % Cu. El Galeno also contains a leached cap that extends approximately 10 m below the surface.

D.5.4 Metal Grade versus Lithology

Average metal grades for the major lithological units identified in logged drill core have been calculated to help understand metal distribution. Contacts between the five major lithological units, i.e. the host sedimentary rocks and the four intrusive phases, were used to divide seven logged drill cores (GA-04, GN-36, GN-37, GN-39, GN-41, GN-42, GN-50) in to the five major rock units. Au, Cu, Mo, Ag, Pb and Zn assay data (Appendix D2) for each of the lithological units were added. The average and standard deviation of the five rock types were calculated for the six metals (Table 1). The total length of each lithological unit intersected in core was also added. The dyke and hydrothermal breccia units were rare in drill core and represent only a few metres of assay data analyses. Therefore, average metals grades for these units have been ignored due to a lack of data for comparison to the other rock units. Drill core GN-39 intersects all five lithological units and has been used to assess the correlation between the metals.

There is a considerable variation in metal grades between the five lithological units (Fig. 12). The standard deviations are mostly high and illustrate the heterogeneity of metal grade throughout each of the units. The highest average Au grades are associated with the P2 porphyry, followed by the P1 porphyry and host rock, and finally

Table 1**:** Average metal grades and standard deviation for identified lithological units in section A-A[1] at Galeno

	Host Rock		**P1 Porphyry**		**P2 Porphyry**		**P3 Porphyry**		**MBx Porphyry**	
	694 m		922 m		108 m		288 m		104 m	Total Length of Core
Metals	Avg	Std Dev	Avg	Std Dev	Avg	Std Dev	Avg	Std Dev	Avg	Std Dev
Au (g/t)	0.10	0.10	0.11	0.13	0.14	0.11	0.04	0.03	0.05	0.05
Cu (%)	0.49	0.26	0.22	0.25	0.32	0.28	0.06	0.04	0.10	0.06
Mo (ppm)	128.6	89.3	82.6	111.6	61.1	46.3	43.8	107.7	48.3	37.4
Ag (ppm)	3.75	3.97	1.66	1.61	1.34	0.79	2.16	5.23	1.81	0.99
Pb (ppm)	90.1	401.0	37.1	65.1	17.9	17.7	100.1	357.9	11.8	8.5
Zn (ppm)	191.7	661.6	76.7	121.7	44.1	34.4	121.3	195.5	41.1	21.0

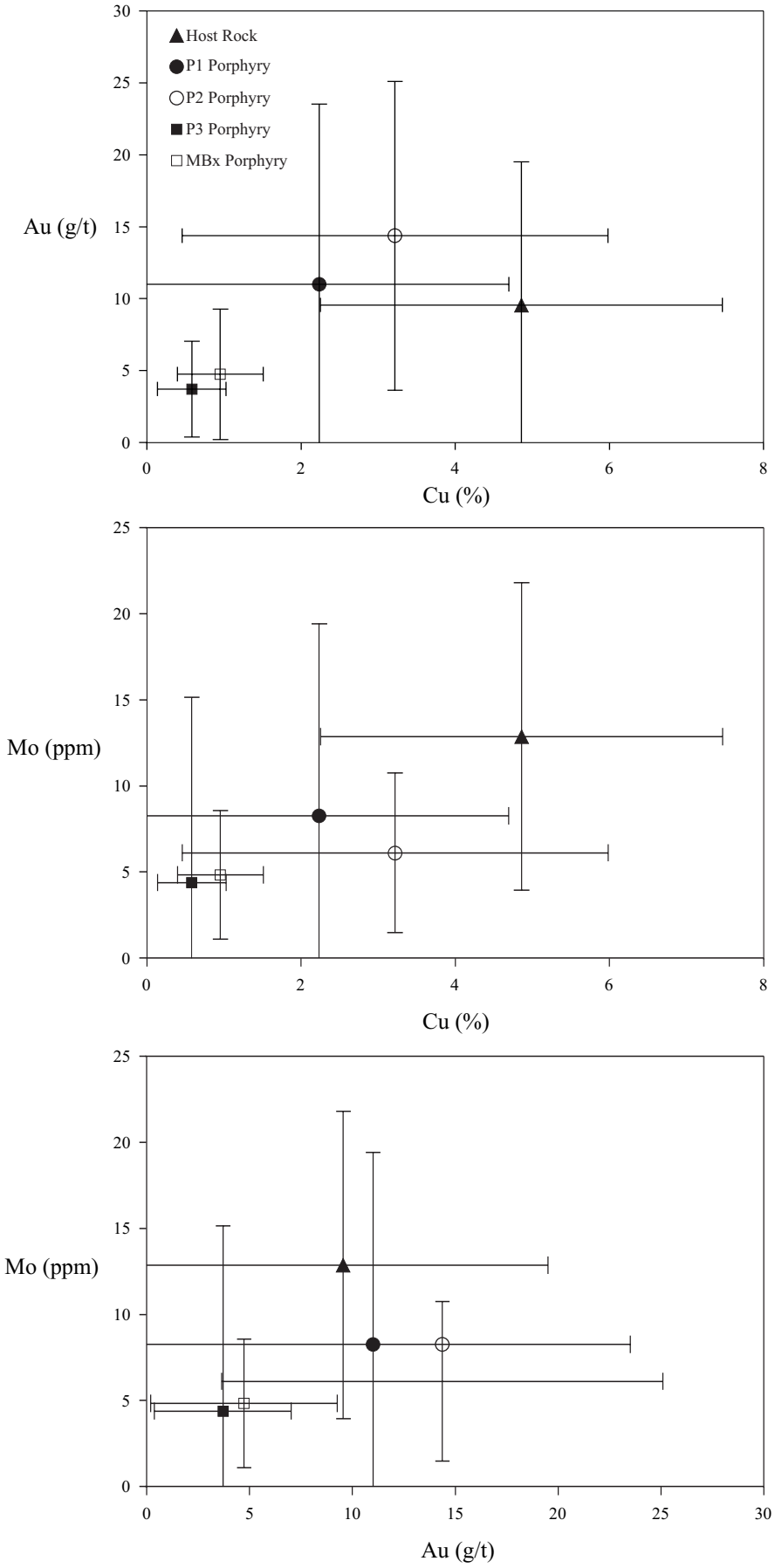

Fig. 12. Plots of average Au vs. Cu and Mo vs. Cu with standard deviation bars from assay data of drill core DDH-GN-39 (refer to Fig. 5).

by the youngest two intrusive phases that are generally poorly mineralised. High Au grades in the P2 porphyry were dominantly intersected toward the centre of the porphyry system. However, high grades are not observed within the same intrusive phase along the outer margins of the complex. High average Cu grades are associated with the oldest two intrusive units (P1 and P2) and extend a few metres into the host rock (Fig. 10), with the final two intrusive phases containing substantially lower grades. A large proportion of the highest Cu grades are located within a supergene enrichment blanket (Fig. 10), although the younger intrusions (P3 and MBx) contain only slightly lower hypogene Cu grades than P1 and P2 intrusions. Low Cu grades were intersected in all lithological units at depth. The host sedimentary rocks contain the highest Mo grades that tend to be spatially restricted along its contacts with the P1 porphyry (see D.5.3), which also contains elevated Mo. The remaining intrusions (P2 – MBx) contain less than half the average Mo grade of the mineralised sedimentary units. The host rocks and P3 porphyry contain the highest Ag, Pb and Zn grades (Appendix D2).

D.5.5 Interpretation of the El Galeno Deposit

Previous interpretations of El Galeno geology include a complex series of stratigraphically controlled sills and laccoliths that intruded along bedding planes or zones of weakness (Hammond, 1998). Recently, Sillitoe (2000a) suggested that several small, vertical, annular dykes intruded an early porphyry body that contains the majority of hypogene mineralisation. Based on observations from this study a revised version of the Sillitoe (2000a) model is presented for the El Galeno deposit.

Emplacement of the principal and earliest porphyry occurred at the intersection of a regional structure crosscut by an oblique secondary structure. The P1 porphyry is elliptical in plan with a northwest trend, similar to the localised structural fabric. Contacts between the intrusion and host rocks are vertical suggesting the intrusive body is an elongate vertical stock. These features indicate that emplacement of the principal El Galeno porphyry (P1) was dominantly structurally-controlled.

Early Mo precipitation occurred along the contacts of the P1 porphyry and host rocks. Candela and Piccoli (1995) showed that at low initial water content and a low

Cl/water ratio, Mo is preferentially partitioned from the melt into exsolved fluid compared to Cu. This suggests early Mo mineralisation is temporally associated with emplacement of the oldest and driest porphyry. Main stage Cu and Au deposition occurred during, or shortly after emplacement of the P2 porphyry, towards the core of the complex where temperatures would have been elevated. A pervasive quartz-magnetite alteration at depth and towards the core of the P1 porphyry possibly developed contemporaneously with emplacement of the P2 porphyry. Both the P1 and P2 porphyries have well-developed potassic alteration hosting modest hypogene mineralisation. The younger intrusions (P3 and MBx porphyries) are mostly evident in drill core, have potassic and phyllic alteration phases, and contain the lowest metal grades. These stocks are poorly mineralised and have a lower abundance of quartz stockwork than the earlier P1 and P2 porphyries. These intrusions are inferred to be late- to post-mineralisation. A substantial proportion of the higher Cu grades are associated with a supergene enrichment zone that extends up to 150 m beneath a thin leached cap. Sillitoe (2000a) suggested late glaciation might have removed a significant proportion of the leached cap and possibly a section of the immediately underlying sulphide enrichment zone.

D.6 Michiquillay

Michiquillay is a Cu-Au-Mo intrusive porphyry system with an indicated resource of 631 Mt at 0.69 % Cu, 0.15 g/t Au and between 100 to 200 ppm Mo with a supergene enrichment zone containing an estimated resource of 46.2 Mt at 1.15 % Cu (McInnes, 1997). The Michiquillay porphyry contains a leached cap (varying from a few metres up to 150 m thick) that overlies a secondary enrichment blanket (1.15 % Cu) extending up to a further 80 m. Exposures of the mineralised complex occur at altitudes from 3,500 to 3,750 m (Fig. 13).

Extensive mapping and drilling in the mid 1970's by the Metal Mining Agency (MMA) defined the dimensions of the intrusive complex as being approximately 5 km in length and 1.5 km wide (Fig. 13). The main intrusive body is roughly parallel to the local NW structural trend. Laughlin *et al*. (1968) dated two intrusions in the Michiquillay region using the K-Ar technique. These include a quartz-biotite monzonite

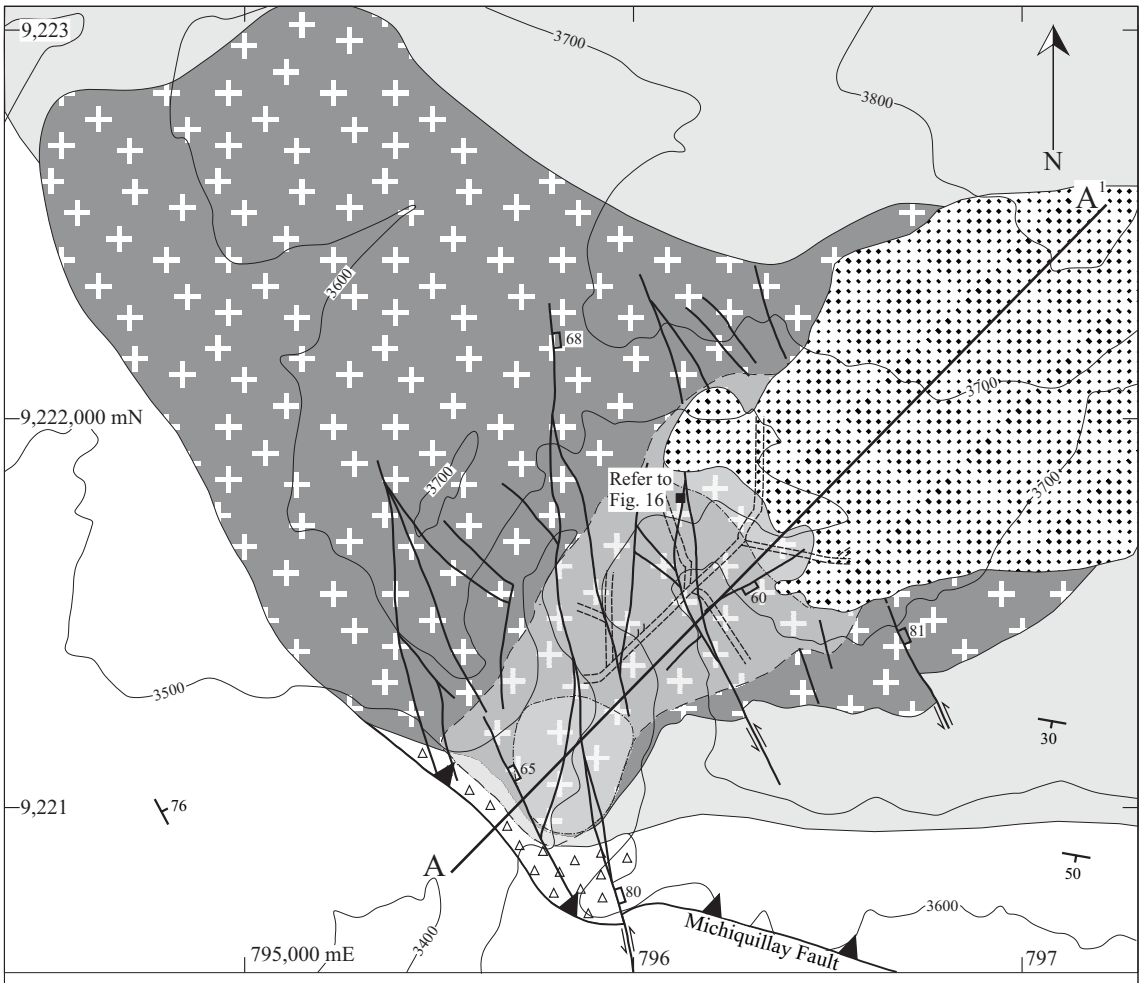

Fig. 13. Simplified geological map of the Michiquillay prospect [modified from previous mapping by MMA (1975)].

from the Michiquillay prospect that yielded an age of 20.6 ± 0.6 Ma (biotite) and a quartz-hornblende monzonite from the Michiquillay suite to the north that produced an age of 46.4 ± 1.8 Ma (hornblende). Llosa *et al*. (1996) obtained an age date of 18.8 ± 1.6 Ma (magmatic biotite) from an intrusion at the Michiquillay prospect also using the K-Ar technique. New $^{40}Ar/^{39}Ar$ age data (Section A) indicate emplacement of a synmineralisation stock at the Michiquillay prospect occurred at 19.77 ± 0.05 Ma. Whilst to the north of the prospect, a barren intrusion was emplaced at 20.6 ± 0.14 Ma (Section A). This indicates synmineralisation stocks at the deposit are slightly younger than unmineralised intrusions to the north.

D.6.1 Lithology

The Michiquillay intrusive centre is hosted within quartzite units to the north and limestone units to the south (Fig.13). At least two major intrusive phases were recognised during drill core logging based on textural evidence. The most common lithology is a medium-grained crowded porphyritic diorite (termed D1) with plagioclase, biotite and hornblende phenocrysts set in a feldspathic groundmass (Fig. 14a). Quartz phenocrysts are rounded, have a low abundance (between 0.5 and 4.0 vol. %) and occur in localised zones. Euhedral plagioclase phenocrysts (An_{42-52}) range from 0.3 to 5.0 mm and are the most abundant mineral (~35-45 vol %). Book-shaped euhedral biotite phenocrysts (~3 vol %) vary from 0.5 to 8 mm and generally contain minor feldspar inclusions. Hornblende phenocrysts (~1-3 vol %) are acicular and mostly 0.3 – 1.0 mm in length. Slight variations in grain-size and mineral abundance occur throughout the intrusive body, although no clear truncations or crosscutting relationships were observed making it difficult to distinguish discrete intrusive phases. Hollister and Sirvas (1974) referred to this as a quartz-biotite monzonite. However, petrographic evidence indicates primary feldspar phenocrysts are plagioclase and primary hornblende grains have been replaced by secondary biotite. Therefore, it is suggested this intrusive unit be classified as a biotite-hornblende diorite.

The second intrusive phase is weakly porphyritic and characterised by low vein abundance and intense biotite alteration (Fig. 14b-c). This medium- to fine-grained intrusive phase dominantly contains euhedral plagioclase phenocrysts (~15 vol %), plus

Fig. 14. Photographs of intrusive units, alteration and mineralisation features at Michiquillay. (a) The D1 porphyry consists of plagioclase, biotite and hornblende phenocrysts with a feldspathic groundmass. The groundmass has been partially to strongly overprinted by hydrothermal biotite (dark grey bottom left). Minor chalcopyrite (middle top) and pyrite (top right) is also present. H-22 176 m. (b) Medium-grained crowded D1 porphyry (left) truncated by a fine-grained dyke (right). Both intrusions contain minor quartz stockwork. J-20 170 m. (c) A dyke with plagioclase and biotite phenocrysts set in a groundmass that has been intensely replaced by hydrothermal biotite. Late pyrite and hematite veins crosscut the dyke. J-20 178.5 m. (d) Chalcopyrite and molybdenite mineralisation in a quartz vein. J-20 333.3 m. (e) Late pyrite veins with quartz-sericite halos crosscut the potassic altered D1 porphyry. I-23 268 m. (f) Quartz-sericite alteration has destructively replaced most primary igneous textures, although some grain boundaries are evident. Late thick pyrite veins are associated with the quartz-sericite alteration. L17.5 288 m.

THE IMAGES ON THIS PAGE HAVE BEEN REMOVED DUE TO COPYRIGHT RESTRICTIONS

biotised hornblende phenocrysts and euhedral biotite books (Fig. 14b). This second intrusive phase form sheets that range in thickness from 1 to 6 m (Fig. 15a). The dykes crosscut and truncate the potassic-altered main intrusion and contain xenoliths of the altered biotite-hornblende diorite (Fig. 14b). The dykes generally lack a well-developed stockwork. No quenched margins were observed along the rims of xenoliths. The dykes were only observed in the northeastern and southwestern zones of the complex. This phase is inferred to be a series of syn- to late-mineralisation vertical diorite dykes.

D.6.2 Structural Geology

The Michiquillay intrusive complex is located in the hanging wall of a NW-trending back thrust (Fig. 13) that was interpreted by Hollister and Sirvas (1974) to be crosscut by the NE-trending Encañada Fault. The latter fault was not recognised during aerial photo analysis or fieldwork by the author and its existence is suspect. The thrust dips at ~60^{o} towards the NE and is referred to as the Michiquillay Fault (Hollister and Sirvas, 1974; MMA, 1975). It is characterised by a matrix-supported breccia that contains both quartzite and limestone fragments, though no intrusive fragments were observed. The Michiquillay Fault was not intersected in drill core. However, in the southern zone of the deposit the reoccurrence of stockwork and change from potassic to phyllic alteration toward the bottom of some drill holes is interpreted to indicate the Michiquillay Fault is nearby (Appendix D4). In outcrop, oblique prospect-scale faults crosscut the porphyry deposit and were previously mapped by MMA (1975). These dominantly occur toward the centre of the deposit (Fig. 13) and are recognisable in outcrop by an increase in fracture density toward the central part of the fault zone. The faults are subvertical and dominantly strike either to the NNW or NNE (Section B.5.2).

The NNW-striking prospect-scale faults separate potassic alteration zones in the NE and SW of the complex, and define the outer limit of a strong phyllic alteration zone. An increase in stockwork density was noted along these fault planes (Fig. 16a). Some NNW fault planes contain localised zones of vuggy quartz that are spatially-associated with strong gossan-like oxidation features (Fig. 16b). The NNW-striking faults are the dominant fault set at the deposit and inferred to have strongly influenced

Geology

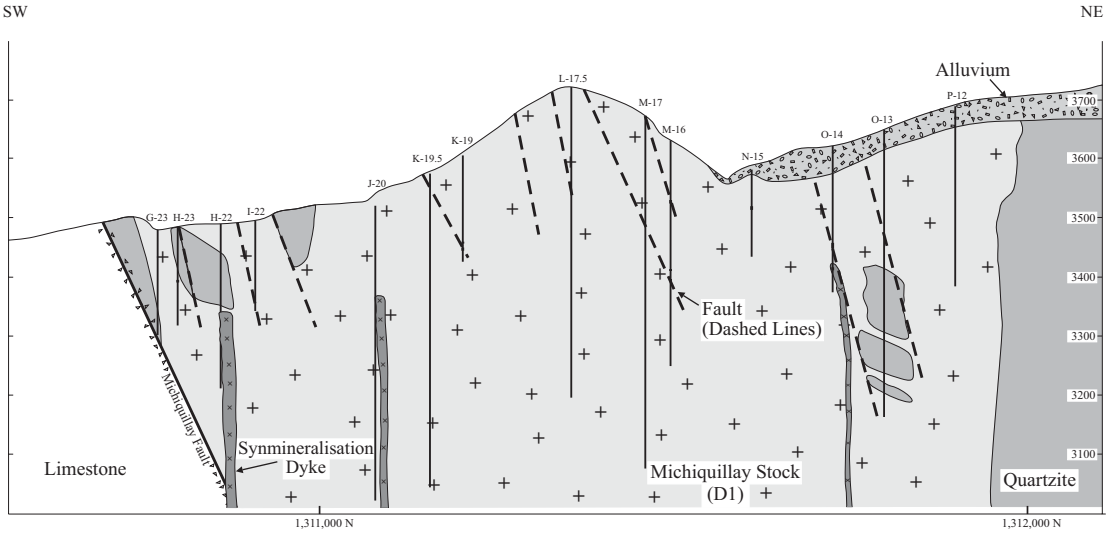

Alteration

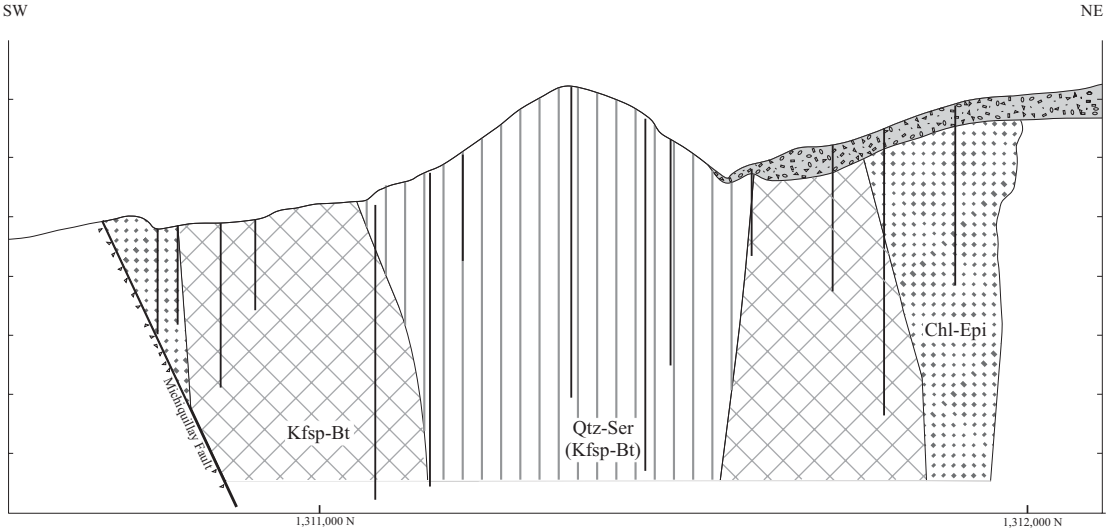

Cu-Distribution

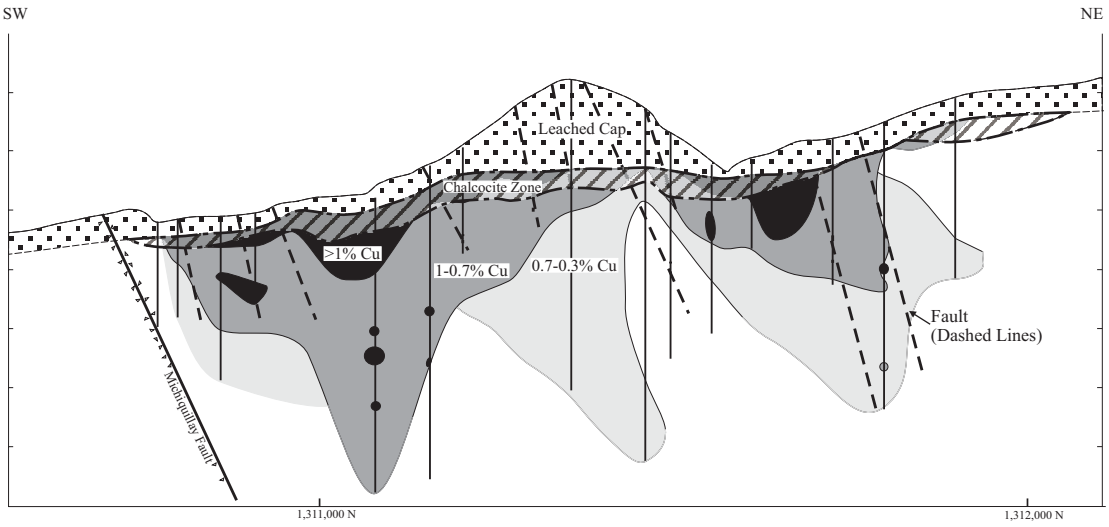

Fig. 15. Section A-A[1] looking NW, showing the major lithological units, alteration and Cu distribution at Michiquillay. Lithology and alteration distribution maps are based on logged drill cores and Cu grade map from assay data (see Appendix D4).

Fig. 16. Images of fault zones observed at Michiquillay. Refer to Fig. 13 for location. (a) Image of a fault plane showing strong quartz stockwork. Late subvertical slickenlines are also evident (centre). (b) A strongly oxidised fault within the D1 porphyry. The centre of the fault zone (bound by dotted lines) contains abundant hematite. Outside the hematite-rich zone, the silicic altered intrusive is strongly fractured.


THE IMAGES ON THIS PAGE HAVE BEEN REMOVED DUE TO
COPYRIGHT RESTRICTIONS

both alteration and mineralisation. Steeply plunging slickenlines on some fault planes (Fig. 16a) indicate late subvertical displacement.

D.6.3 Alteration and Mineralisation

Both intrusive phases contain a well-developed K-feldspar-biotite-quartz-magnetite alteration assemblage. The potassic alteration is strongest in the northeastern and southwestern parts of the prospect (Fig. 15b), but extends only a few metres in the host rock. Surface expressions of the potassic alteration zones have a NE trend (Fig. 13). This alteration is characterised by the replacement of plagioclase by K-feldspar and the precipitation of fine-grained hydrothermal biotite that is strongly developed in the southwestern zone. The northeastern zone contains only moderate biotitisation but stronger K-feldspar-quartz alteration. Despite these slight variations, both the southwestern and northeastern zones display very similar alteration styles. Veins associated with the K silicate alteration include early thin (1-2 mm) wavy magnetite and biotite veins that are crosscut by quartz veins. Hypogene sulphides associated with the potassic alteration include chalcopyrite, molybdenite (Fig. 14d), pyrite and minor bornite. These minerals occur as infill in veins and fractures, as well as disseminated in the groundmass. Microscopic studies by MMA (1975) reported that pyrrhotite and sphalerite also precipitated during this stage. Based on logging results and corresponding assay data (Appendix D4), average hypogene grades for these zones are approximately 0.14 g/t Au and 0.8 % Cu.

Intense quartz-muscovite-pyrite (phyllic) and late kaolinite (argillic) alteration zones occupy the core of the complex (Fig. 15b). Quartz-pyrite veins with muscovite/illite (Appendix D3) halos are observed throughout the intrusive complex and crosscut all veins (Fig. 14e). Intense phyllic alteration has destructively overprinted older textures (Fig. 14f). Intensity of the quartz-muscovite alteration however weakens toward the edges of the core where it has partially replaced potassic-altered rocks. As mentioned above, NNW-striking faults are inferred to have controlled the distribution of these alteration assemblages. Sulphides precipitated during this alteration include large amounts of pyrite (Fig. 14f), plus minor molybdenite and chalcopyrite (McInnes, 1997). MMA (1975) also identified enargite, luzonite and tetrahedrite-tennantite within the

central upper parts of the phyllic alteration zone. Au and Cu grades in this zone (0.08 g/t Au and 0.57 % Cu; Appendix D4) are lower than in the potassic alteration zones.

Michiquillay contains a supergene enrichment zone characterised by covellite and chalcocite replacement of hypogene chalcopyrite (Fig. 15c). Grades associated with this enrichment zone range from 2.2 to 0.5 % Cu, at an average of ~1.09 % Cu (McInnes, 1997). In parts, late clay (argillic) alteration partially to moderately overprints the quartz-muscovite alteration. Clay alteration is spatially associated with fault zones and extends to depths of 100 m below the surface. The composition of the clays was determined as kaolinite from X-ray diffraction analysis (Appendix D3). Late development of malachite is evident in both outcrop and on drill core.

D.6.4 Interpretation of the Michiquillay Complex

Based on the findings from this study combined with previous work (Hollister and Sirvas, 1974; MMA, 1975; McInnes, 1997) a revised model of the Michiquillay deposit is presented. Emplacement of the Michiquillay porphyry during early to middle Miocene times (~19.8 Ma) was structurally controlled by the Michiquillay Fault. The existence or significance of the Encañada Fault proposed by Hollister and Sirvas (1974) is unclear. Early potassic alteration developed along a NE trend and was associated with chalcopyrite, pyrite, magnetite, bornite and minor molybdenite mineralisation. Significant hypogene Cu and Au grades are preserved in the northeastern and southwestern potassic alteration zones. Late hydrothermal fluids related to phyllic and argillic alteration were transported along the NNW fault planes and overprinted earlier potassic alteration. An intense phyllic alteration zone located toward the centre of the deposit defines a pyritic-rich, low-grade zone. It is inferred that these late fluids remobilised some Cu and Au associated with early potassic alteration. The deposit contains a supergene enrichment zone located beneath a leached cap of varying thickness.

D.7 Pb Isotope Composition Of Sulphide Minerals

Pb isotope compositions of ores and igneous rocks have been used to infer the source of metals associated with central Andean ($6^{o}S$ to $32^{o}S$) magmatic-hydrothermal ore deposits [refer to Macfarlane (1999) and references therein]. Based on these compositions, Macfarlane *et al*. (1990) and Petersen *et al*. (1993) presented maps of the central Andes that identified three main Pb isotope provinces (Fig. 17). Pb isotope data defining province I are generally less radiogenic and interpreted to reflect a well-mixed sub-Andean mantle enriched by subducted sediment (Barriero, 1984; Macfarlane, 1999). Province III has elevated $^{207}Pb/^{204}Pb$ and $^{206}Pb/^{204}Pb$ values characteristic of upper crustal lead and is inferred to represent melting of an old felsic crust (Pichavant *et al*., 1988). Province II Pb isotope ratios lie between the two previous provinces. Macfarlane *et al*. (1990) interpreted these values to represent varying degrees of mixing between mantle-type (province I) and crustal-type (province III) sources. The Pb isotope compositions of chalcopyrite and pyrite separates from potassic altered synmineralisation intrusions at El Galeno, Michiquillay and Minas Conga were determined to assess for any systematic variation in the source of metals throughout the Cajamarca region. Additionally, chalcopyrite separates from the late poorly mineralised MBx porphyry at El Galeno and pyrite from a quartz-sericite altered intrusion at the Yanacocha mine were also analysed. Duplicate samples were also run for some of the samples. These analyses were conducted at the University of British Columbia and analytical procedures are reported in Appendix D5.

Pb isotope ratios of the sulphide minerals from the deposits display moderate scatter but tend to plot in steep linear trends (Fig. 18a; Table 2). Pyrite from Yanacocha has the least radiogenic Pb, whilst pyrite grains from Minas Conga generally are the most radiogenic. Of particular note, duplicate samples of sulphides show some variation (Table 2) but are generally within analytical error (Appendix D5). These variations in Pb isotope ratios may reflect either sample heterogeneity or thermal fractionation. Heterogeneity between the grains may result from mineral inclusions within the analysed grains. Alternatively, an external fluid or source, possibly from the host carbonate rocks, may cause heterogeneous grain compositions. Variations in Pb isotope compositions due to external fluid contributions, such as the host rocks, have been documented in late-stage sulphides at the Potrerillos deposit in Chile (see Tosdal *et al*.,

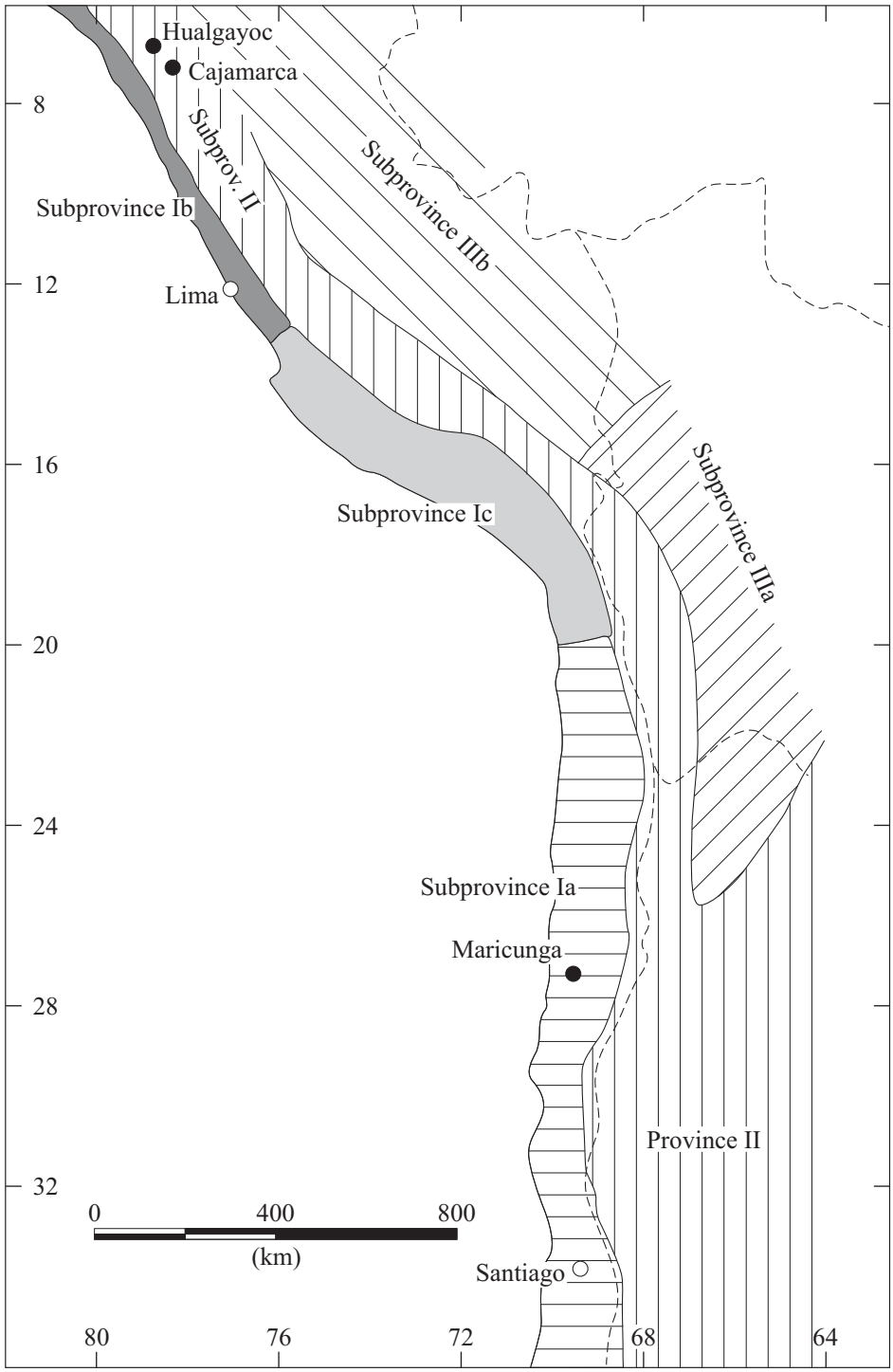

Fig. 17. Pb isotope map of the central Andes showing the provinces as proposed by Macfarlane *et al. (1990)* and Petersen *et al. (1993).*

Fig. 18. A. Plots of Pb isotope ratios for sulphides from mineralised intrusions at the El Galeno (G), Michiquillay (MY), Minas Conga (MC) and Yanacocha deposits in the Cajamarca region. PYR = Pyrite; CCP = Chalcopyrite. B. Pb isotope compositions from previous studies of ores and igneous rocks from the Hualgayoc district (Macfarlane and Petersen, 1990) and fields for the various Andean Pb isotope provinces and subprovinces as defined by Macfarlane *et al*. (1990) and Petersen *et al*. (1993). S/K = average crustal growth curve of Stacey and Kramers (1975).

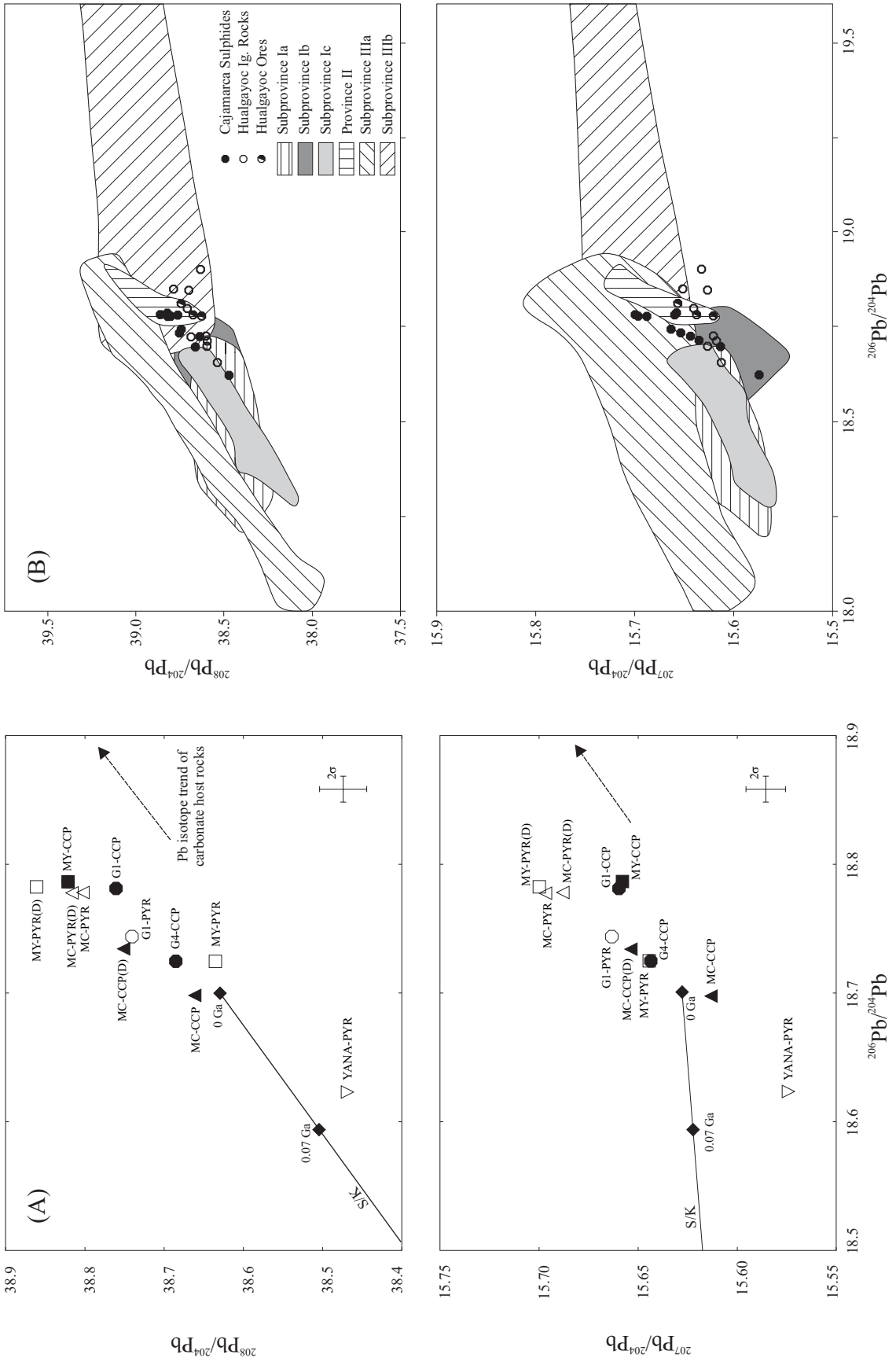
(A)
(B)
MY-PYR(D)
MY-CCP
MC-PYR(D)
MC-PYR
G1-CCP
MC-CCP(D)
G1-PYR
G4-CCP
MY-PYR
MC-CCP
0 Ga
0.07 Ga
S/K
YANA-PYR
Pb isotope trend of carbonate host rocks
2σ
Cajamarca Sulphides
Hualgayoc Ig. Rocks
Hualgayoc Ores
Subprovince Ia
Subprovince Ib
Subprovince Ic
Province II
Subprovince IIIa
Subprovince IIIb
$^{208}Pb/^{204}Pb$
$^{207}Pb/^{204}Pb$
$^{206}Pb/^{204}Pb$

Table 2. Pb isotope compositions of pyrites (PYR) and chalcopyrites (CCP) from mineralised porphyritic intrusions in the Cajamarca region.

Sample No.	Deposit	Drill Core	Depth (m)	Intrusion	Alteration Zone	Sulphide	$^{206}Pb/^{204}Pb$	$^{207}Pb/^{204}Pb$	$^{208}Pb/^{204}Pb$	$^{207}Pb/^{206}Pb$	$^{208}Pb/^{206}Pb$
G1-CCP	Galeno	GN-39	166.1	P1 Porphyry	Potassic	Chalcopyrite	18.7813	15.6597	38.7608	0.8338	2.0638
G1-PYR	Galeno	GN-39	166.1	P1 Porphyry	Potassic	Pyrite	18.7440	15.6633	38.7405	0.8356	2.0668
G4-CCP	Galeno	GN-39	432.0	MBx Porphyry	Potassic	Chalcopyrite	18.7071	15.6348	38.6853	0.8358	2.0680
MY-PYR	Michiquillay	J-20	346.7	D1 Porphyry	Potassic	Pyrite	18.7248	15.6439	38.6349	0.8355	2.0633
MY-PYR(D)	Michiquillay	J-20	346.7	D1 Porphyry	Potassic	Pyrite	18.7826	15.7000	38.8606	0.8359	2.0690
MY-CCP	Michiquillay	J-20	346.7	D1 Porphyry	Potassic	Chalcopyrite	18.7865	15.6577	38.8215	0.8335	2.0665
YANA-PYR	Yanacocha	CLL-05	569.0	Tonalite	Quartz-Sericite	Pyrite	18.6234	15.5742	38.4688	0.8363	2.0656
MC-CCP	Minas Conga	H-1	151.5	Main Diorite	Potassic	Chalcopyrite	18.6980	15.6132	38.6605	0.8350	2.0676
MC-CCP(D)	Minas Conga	H-1	151.5	Main Diorite	Potassic	Chalcopyrite	18.7342	15.6536	38.7507	0.8356	2.0685
MC-PYR	Minas Conga	H-1	151.5	Main Diorite	Potassic	Pyrite	18.7778	15.6968	38.8161	0.8359	2.0672
MC-PYR(D)	Minas Conga	H-1	151.5	Main Diorite	Potassic	Pyrite	18.7781	15.6878	38.8013	0.8355	2.0664

Results have been normalized using a fractionation factor of 0.15% based on multiple analyses of NBS981 standard lead, and the values in Thirlwall (2000).

(D) = duplicate samples

1999 and references therein). Sedimentary host rocks in the Cajamarca region have more radiogenic Pb and flatter Pb ratio trends compared to sulphides (Fig. 18a: Macfarlane, 1999). Therefore, the host rock compositions cannot solely account for the sulphide steep linear trend (Fig. 18a). Finally, analytical error, such as thermal fractionation in the mass spectrometer, may also account for some of the variation in the data (Tosdal, *pers. commun*., 2002).

Regionally, pyrite from Yanacocha has the least radiogenic Pb and plots toward the nonradiogenic end of the province Ib array (Fig. 18b). Pyrite from Michiquillay, and chalcopyrite from the MBx porphyry at El Galeno also lie at the nonradiogenic end of the data and within the province Ib array. Chalcopyrites from the main intrusions at El Galeno, Michiquillay and Minas Conga have very similar Pb isotope compositions that plot between the end members of the province I and II arrays. In contrast, pyrites from Minas Conga and possibly Michiquillay have elevated $^{208}Pb/^{204}Pb$ and $^{207}Pb/^{204}Pb$ values. These samples plot toward the radiogenic end of the province II array (Fig.18b). With the exception of pyrite from Minas Conga and Michiquillay(?), these results overlap with Pb isotope compositions of ores and igneous rocks from the Hualgayoc region (Macfarlane and Petersen, 1990).

D.8 Discussion

D.8.1 Variations in Mineralised Porphyry Complexes

The Cajamarca district hosts a number of mineralised porphyry and high-sulphidation systems that display varying mineralisation and alteration styles. Three mineralised porphyry associations, El Galeno (Cu-Au-Mo porphyry), Michiquillay (Cu-Au-Mo porphyry) and the Chailhuagon-Perol (Au-Cu) porphyry complexes at Minas Conga (Llosa and Veliz, 2000) were emplaced within 6 m.y. of each other but have significantly different metal grades (Table 3). Turner (1999) suggested one of the principal differences between the various high-sulphidation systems in the Cajamarca region relates to level of erosion. He argued that the Yanacocha Au mine represents a high-level epithermal system characterised by phreatic breccias and has a poorly-understood structural control, whereas Sipán and La Zanja are relatively deeply-eroded

Table 3: Summary of the El Galeno, Michiquillay and Minas Conga porphyry centres.

	El Galeno[1]	**Michiquillay**[1, 2]	**Chailhuagon (Minas Conga)**[3, 1]	**Perol (Minas Conga)**[3]
Metal Association	Cu-Au-Mo	Cu-Au-Mo	Au-Cu	Au-Cu
Resource	486Mt @ 0.57% Cu + 0.14g/t Au	631Mt @ 0.69% Cu + 0.15g/t Au	102Mt @ 0.9g/t Au + 0.30% Cu	428 Mt @ 0.8g/t Au + 0.31% Cu
Age (Ma)	17.5 – 16.5	20.6 – 19.8	23.2 – 17.1	23.2 – 17.1
Intrusion Type	Hornblende-Biotite Diorite	Hornblende-Biotite Diorite	Hornblende-Biotite Diorite	Hornblende-Biotite Diorite
No. Intrusions Recognised	4	2	2	3
Dimensions of Principal Intrusive	1250 x 600 m (NW oriented)	5000 x 1500 m (NW oriented)	2000 x 500 m (N-S oriented)	1600 x 650 m (NW oriented)
Host Rock Type	Qtzte, Sst and Sh	Lst and Qtzte	Lst and Marl	Lst, Marl and MGD
Elevation (m.a.s.l.)	3,850 – 4,000	3,500 – 3,750	3,840 – 3,900	3,870 – 3,960
Structural Control of Porphyry Emplacement	Located at the intersection of several structures	Emplaced within the hanging wall of reverse fault	Located at the intersection of N- and NW-trending faults	NW-trending Perol Thrust Fault
Brecciation	Minor hydrothermal breccia, post-mineralisation magmatic breccia	Minor magmatic breccia, generally absent	Absent	Absent
Principal Alteration Phases	K, QM, QS, CbEF	K, M, QS, E, Cl	K(+M), QS, Skn, Q, CbE	K(+M), QS, Skn, AA
Quartz Stockwork	Moderate – Strong	Moderate – Strong	Strong	Strong-moderate
Controls on Mineralisation	Dominantly Intrusion Related	NNW faults and NE alteration trend	Intrusion and Vein Related	Intrusion and Vein Related
Main Hypogene Sulphides	Py, Ccp, Mo	Ccp, Pyr, Mo	Ccp, Bn, Py	Ccp, Bn, Py
Supergene Blanket	Present (0-120 m)	Present (0-40 m)	Absent	Poorly Developed (<50 m)
Supergene Sulphides	Cc, Cv	Cc, Cv	Cc, Cv	Cc, Cv
Leached Cap	Thin (<10 m)	Moderate-Thick (up to 80 m)	Absent	Absent

Rock Types: Qtzte = quartzite; Sst = sandstone; Sh = shale; Lst = limestone; MGD = microgranodiorite
Alteration Phases: K = potassic; Q = quartz/silicic; M = magnetite; S = sericite; Skn = skarn; AA = advanced argillic; Cb = carbonate; E = epidote; F = fluorite; Cl = clay
Sulphides: Py = pyrite; Ccp = chalcopyrite; Mo = molybdenite; Bn = bornite; Cc = chalcocite; Cv = Covellite
1 = This Study; 2 = MMA (1975), McInnes, (1997); 3 = Llosa and Veliz (2000)

systems where magmatic plus hydrothermal breccias predominate and structural controls are more clearly recognised. The following paragraphs compares and contrasts early Miocene porphyry-related deposits in the Cajamarca region. The aim of this is to identify the key process that caused the variation in metal grades amongst the deposits.

El Galeno is dominantly hosted in quartzites, Michiquillay in both quartzites and limestones, whereas the Minas Conga systems are mostly hosted in limestones and marls. Host rocks with low permeability, such as marbleised limestone, minimise lateral flow of hydrothermal fluids, thereby focusing metalliferous fluids to the host intrusion and possibly increasing metal concentrations (Sillitoe, 2000b). El Galeno, Michiquillay and Chailhuagon deposits consist of early to middle Miocene hornblende-biotite diorites that are geochemically very similar (Section C.12.1). Chailhuagon is the oldest complex and the main porphyritic stock was emplaced ~23.2 Ma (Llosa *et al*., 1996). Drilling at both Chailhuagon and Perol has defined post-mineralisation stocks at depth that significantly reduces the Au-Cu grade of both deposits (Llosa and Veliz, 2000). Michiquillay contains two recognisable synmineralisation intrusions that were emplaced at approximately 19.8 Ma (Section A). El Galeno is the youngest system (17.5 – 16.5 Ma) and has the most complex intrusive history, with at least four intrusive phases present. The earliest two intrusions at El Galeno are synmineralisation, whilst the final two represent late- to post-mineralisation porphyries. Post-mineralisation low-grade or barren stocks are however common features of both Au-rich and Cu-Au-Mo porphyry deposits (e.g. Maricunga belt, Vila and Sillitoe, 1991; Bajo de la Alumbrera, Ulrich and Heinrich, 2001; Sillitoe, 2000b).

Multiple alteration stages at El Galeno were temporally related to the emplacement of different intrusions. The earliest two porphyries are characterised by K-feldspar-biotite alteration and an intense quartz-magnetite alteration at depth. Potassic alteration is weakly overprinted by quartz-muscovite alteration associated with emplacement of later intrusions. At Michiquillay, the distribution of the two dominant alteration assemblages, i.e. potassic and phyllic, was controlled by NNW-trending prospect-scale faults. Intense potassic alteration consisting of K-feldspar, biotite and widespread magnetite defines the Chailhuagon main porphyritic stock. Both Galeno and Michiquillay lack widespread hydrothermal magnetite throughout the deposit. Au-rich porphyry deposits, such as Grasberg (Meinert *et al*., 1997; Pollard and Taylor, 2002),

Far South East (Hedenquist *et al*., 1998) and Bajo de la Alumbrera (Ulrich and Heinrich, 2001), are commonly characterised by abundant hydrothermal magnetite associated with an early potassic alteration (Clark and Arancibia, 1995; Sillitoe, 2000b). All three mineralised centres in the Cajamarca district contain weak silicic, propylitic and late carbonate alteration. Skarn alteration is also evident at Perol and to a lesser extent at Chailhuagon.

Significant differences between the three mineralised porphyry centres relate to the hypogene sulphide assemblage and the presence or absence of a well-developed phyllic alteration. At El Galeno, hypogene Cu and Au grades are temporally and spatially associated with the two earliest intrusions. Potassic alteration zones in these intrusions have a high quartz stockwork density. Pyrite, molybdenite and to a slightly lesser extent chalcopyrite largely form the hypogene sulphide assemblage. At Michiquillay, high hypogene grades occupy zones of intense potassic alteration and are associated with chalcopyrite, pyrite, molybdenite and minor bornite. Late-stage fluids transported along NNW-trending faults at the prospect resulted in development of a low-grade, pyrite-rich phyllic core that overprinted the early potassic alteration. Gammons and Williams-Jones (1997) suggest late-stage fluids associated with phyllic overprinting have the potential to remobilise significant quantities of Au and Cu. Such a scenario is proposed for Michiquillay, where late-stage fluids remobilised early potassic alteration-related Cu and Au mineralisation away from the centre of the deposit. In contrast to Michiquillay and El Galeno, high metal grades at Chailhuagon are deficient in molybdenum. High hypogene Au and Cu grades are characterised by abundant bornite, magnetite and chalcopyrite. A strong association between gold and bornite mineralisation has been documented at other Au-rich porphyry deposits such as Bingham (Ballantyne *et al*., 1997) and Grasberg (Rubin and Kyle, 1997). However, where bornite is absent or chalcopyrite is more abundant than bornite, gold distribution is generally closely associated with chalcopyrite (Ballantyne *et al*., 1997, Ulrich and Heinrich, 2002; Kesler *et al*., 2002). Experimental studies of Au distribution for high temperature (400^{o} to 700^{o}C) porphyry copper deposits indicate that bornite is the dominant host of Au at temperatures of 700^{o}C or greater (Fig. 19; Simon *et al*., 2000). Additionally, chalcopyrite preferentially precipitates over bornite and magnetite at lower temperatures and oxygen fugacity. These authors also showed that when

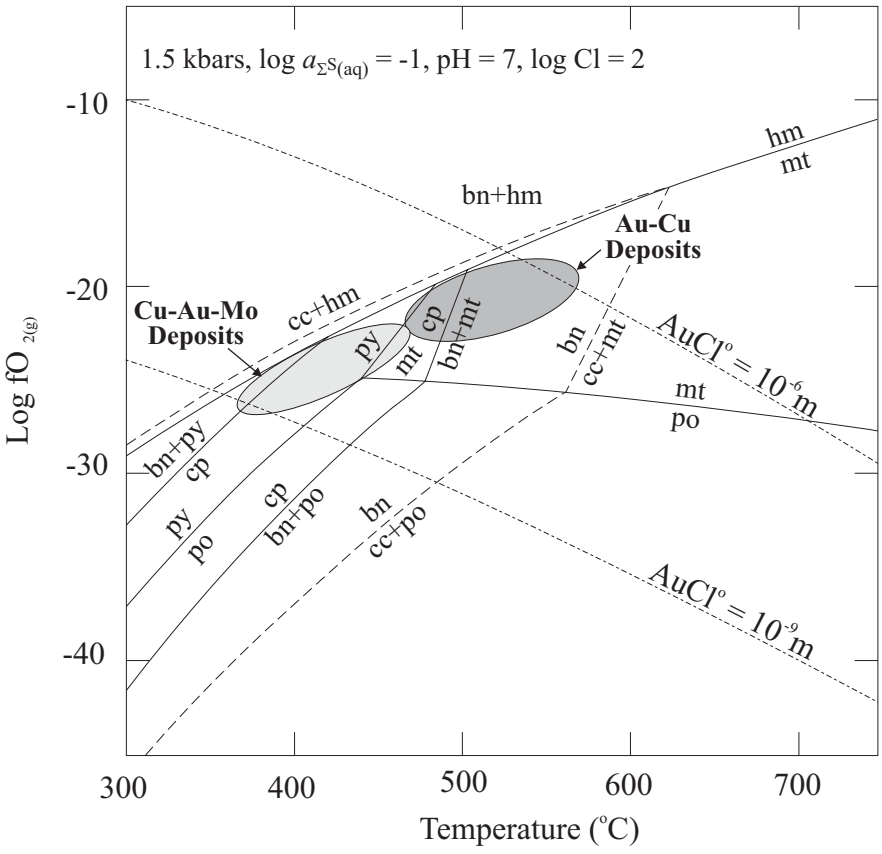

Fig. 19. Temperature-oxygen fugacity diagram for the Fe-Cu-S-O system with contours for solubility $AuCl^{o}$ (adapted from Simon *et al*. 2000). Main stage mineralisation at the Au-Cu type deposits, such as Chailhuagon and Perol, are inferred to have formed at higher temperatures and oxygen fugacity than Cu-Au-Mo type deposits, such as Michiquillay and El Galeno.

experimentally equilibrated with Au, chalcopyrite was found to contain one order of magnitude less Au than bornite.

The highest Cu grades at El Galeno are spatially-restricted to a secondary enrichment blanket that may have been partially removed during glaciation. Michiquillay also contains supergene enrichment zone of ~45 m thickness that is located beneath a moderately thick (up to 80 m) leached cap. In contrast, supergene enrichment and chalcocite-covellite replacement is very rare at Minas Conga.

Pb isotope compositions of sulphides from potassic alteration zones at three of the deposits, El Galeno, Michiquillay and Chailhuagon, plot on steep linear trend that suggests a common deep source. Pb isotope ratios of chalcopyrite from the Au-rich Chailhuagon deposit lie toward the centre of the Andean province I array. Sulphide Pb ratios from El Galeno and Michiquillay plot within the radiogenic end of the province I isotope array and overlap with previous Pb isotope compositions of ores and igneous rocks from the Hualgayoc region (Macfarlane and Petersen, 1990). Chalcopyrite from the Chailhuagon intrusion extends in to the radiogenic end of the Andean province II array. These results are consistent with a deep, possibly upper sub-Andean mantle, source that has been enriched by subducted sediment and undergone limited mixing of upper crustal material (Macfarlane, 1999).

D.9 Conclusion

The Cajamarca region hosts a number of significant Miocene porphyry-related deposits, including El Galeno (Cu-Au-Mo), Michiquillay (Cu-Au-Mo) and Minas Conga (Au-Cu). Despite significantly varying in Au and Cu concentrations, synmineralisation intrusions at these deposits have similar geochemical compositions and trends (Section C). New sulphide Pb isotope data show some variation but are consistent with a common mantle-dominated source. Based on observations presented in this section, a key difference between Au and Cu concentrations at the deposits is proposed to be the physio-chemical conditions associated with early stage hypogene mineralisation. Deposits at the Au-rich Minas Conga centre have a well-developed potassic alteration zone comprised of ubiquitous hydrothermal magnetite and a high

temperature-oxygen fugacity hypogene sulphide assemblage dominated by bornite and chalcopyrite. These features conform to a generalised model for most Au-rich porphyry-related deposits found along the Andes and worldwide (Sillitoe, 2000b). Michiquillay and El Galeno are Cu-Au-Mo deposits that fit to generalised model for Andean porphyry Cu deposits proposed by Sillitoe (1988). These deposits contain an early potassic alteration overprinted by phyllic alteration, and in contrast to Minas Conga, lower temperature hypogene sulphide assemblages characterised by chalcopyrite and pyrite. Other factors that influenced metal grades between the deposits may include the occurrence of late-stage fluids resulting in development of an intense phyllic alteration and remobilisation of early potassic alteration-related metals, presence of widespread hydrothermal magnetite, complexity of intrusive history and host rock type.